Familial ALS/FTD-associated RNA-Binding deficient TDP-43 mutants cause neuronal and synaptic dysregulation *in vitro*

Molly Magarotto[1], Richard T Gawne[1,2], Gabriele Vilkaite[1], Andrew S Mason[1,2], Han-Jou Chen[1,*]

1: Department of Biology and York Biomedical Research Institute, University of York, Wentworth Way, YO10 5DD, York, UK

2: Jack Birch Unit for Molecular Carcinogenesis, Department of Biology and York Biomedical Research Institute, University of York, Wentworth Way, York YO10 5DD, UK

*Corresponding authors:

Han-Jou Chen, York Biomedical Research Institute, Department of Biology, University of York, Wentworth Way, YO10 5DD, York, UK

(T) +44 1904328729

Email: han-jou.chen@york.ac.uk

Abstract

TDP-43 is an RNA-binding protein constituting the pathological inclusions observed in ~95% of ALS and ~50% of FTD patients. In ALS and FTD, TDP-43 mislocalises to the cytoplasm and forms insoluble, hyperphosphorylated and ubiquitinated aggregates that enhance cytotoxicity and contribute to neurodegeneration. Despite its primary role as an RNA/DNA-binding protein, how RNA-binding deficiencies contribute to disease onset and progression is little understood. Among many identified familial mutations in TDP-43 causing ALS/FTD, only two mutations cause an RNA-binding deficiency, K181E and K263E. In this study, we used CRISPR/Cas9 to knock-in the two disease-linked RNA-binding deficient mutations in SH-SY5Y cells, generating both homozygous and heterozygous versions of the mutant TDP-43 to investigate TDP-43-mediated neuronal disruption. Significant changes were identified in the transcriptomic profiles of these cells, in particular, between K181E homozygous and heterozygous cells, with the most affected genes involved in neuronal differentiation and synaptic pathways. This result was validated in cell studies where the neuronal differentiation efficiency and neurite morphology were compromised in TDP-43 cells compared to unmodified control. Interestingly, divergent neuronal regulation was observed in K181E-TDP-43 homozygous and heterozygous cells, suggesting a more complex signalling network associated with TDP-43 genotypes and expression level which warrants further study. Overall, our data using cell models expressing the ALS/FTD disease-causing RNA-binding deficient TDP-43 mutations at endogenous levels show a robust impact on transcriptomic profiles at the whole gene and transcript isoform level that compromise neuronal differentiation and processing, providing further insights on TDP-43-mediated neurodegeneration.

Keywords

TDP-43

Neurodegeneration

Amyotrophic Lateral Sclerosis

Frontotemporal Dementia

RNA-binding protein

Introduction

TDP-43 is a prominent protein critically involved in neurodegenerative conditions including Amyotrophic Lateral Sclerosis (ALS), Frontotemporal Dementia (FTD) and Alzheimer's Disorder (AD). It constitutes the pathological inclusions, known as TDP-43 proteinopathy, observed in ~95% of ALS, ~50% of FTD (1), and in severe forms of AD (2,3). As a DNA/RNA-binding protein, TDP-43 is a key regulator of RNA metabolism and processes such as transcription and splicing, and the maintenance and transport of mRNAs (4,5). In disease, TDP-43 mislocalises to the cytoplasm and forms insoluble, hyperphosphorylated and ubiquitinated aggregates (1,6) contributing to enhanced cytotoxicity that is directly linked to neurodegeneration and disease development (1,7,8). In addition to the cytotoxicity directly caused by the aggregates, the sequestering of TDP-43 in aggregates also reduces the levels of functional soluble TDP-43 in the cell, impacting the expression of target genes causing a cascade effect that eventually compromises neuronal health (9,10).

Despite TDP-43's prominent role in RNA regulation, this process in disease has been largely overlooked due to hot spots of disease-linked TDP-43 mutations in the aggregation-prone C-terminal of the protein, away from the RNA recognition motifs (RRMs) (11). Currently, TDP-43 is known to directly bind to around 6000 pre-mRNAs in the nervous system, regulating their expression and splicing (4,12). Some of the known targets of TDP-43 such as *STMN2* and *UNC13A* are known to contribute to ALS pathology when misregulated (13–16). The reduction of the full-length *STMN2* and induction of truncated *STMN2* caused by TDP-43 depletion leads to reduced neurite complexity and motor neuron health (15,17). Reduction of *UNC13A* expression causes disruptions in synapse function, contributing to ALS/FTD pathology (13,16). These studies demonstrate that TDP-43 plays a pivotal role in maintaining neuronal health via orchestration of a large network of downstream targets. Many studies have so far employed TDP-43 knockdown as a model. While knockdowns can mimic TDP-43 loss of function, global protein loss does not fully recapitulate the complexity of the disease genetics and pathology.

To further investigate the impact of TDP-43 RNA dysregulation, specifically RNA-binding by TDP-43 in a disease-relevant model, we focus on two disease-associated TDP-43 mutations, K181E and K263E. Both mutations are identified in ALS and FTD affected families, linked to the disease phenotypes in an autosomal dominant inheritance pattern (10,18). These mutations are located adjacent to the RNA recognition motifs (RRMs) of TDP-43 and disrupt the binding of TDP-43 to target RNA (10), causing TDP-43 protein to form highly insoluble and phosphorylated nuclear aggregates (10,19). RNA-binding deficient TDP-43-induced nuclear aggregates can sequester endogenous wild-type TDP-43 (10) and potentially other proteins and RNAs, driving a decline in cellular health.

In this study, we used CRISPR/Cas9 to introduce point mutations K181E and K263E into the *TARDBP* gene of human neuroblastoma cell line, SH-SY5Y. Clones of cells carrying either heterozygous and homozygous mutations were generated, which showed the expected change in the splicing pattern of TDP-43 target RNA *PolDip3* as seen in previous studies (10,20). Transcriptomic comparison revealed significant gene expression differences in neuronal and synaptic genes between K181E-TDP-43 homozygous and heterozygous cells compared to wild-type control. Interestingly, many of these genes are up-regulated in K181E-TDP heterozygous cells but down-regulated in K181E-TDP homozygous cells. This finding is validated functionally in the observation of differing degrees of efficiency in neuronal differentiation and neurite growth in the cells carrying the disease-linked RNA-binding deficient mutant TDP-43 with heterozygotes pre-disposed to differentiate and homozygotes unable to differentiate.

Methods and Materials

CRISPR/Cas9-mediated TDP-43 genome editing via nucleofection

GuideRNA (gRNA) and HDR template (ssODN) (Figure 1A) were designed using the IDT Custom Alt-R™ CRISPR-Cas9 guide RNA and Alt-R HDR Design tools (IDT), where its on-target efficiency and off-target cuts were also estimated. The sequence of crRNAs used in this study are: K181E 5'-GACGCAAGTACCTTAGAATT-3', K263E: 5'-ATTGCTATTGTGCTTAGGTT-3'. HDR templates used in this study are K181E 5'-TATGATAGATGGACGATGGTGTGACTGCAAACTTCCTAATTCTGAGGTACTTGCGTCTGTGCTTTGGGAATTTTTGCCAACAAA-3', K263E 5'-ATCATTAAAGGAATCAGCGTTCATATATCCAATGCAGAACCTGAGCACAATAGCAATAGACAGTTAGAAAGAAGTGGAAGATT-3'. 100µM of sequence-specific crRNAs (IDT) were mixed with 100µM of tracrRNA (IDT), heated to 95°C for 5 minutes to form 50µM of gRNA which were subsequently aliquoted and stored at -20°C.

SH-SY5Y cells were cultured using Dulbecco's modified Eagle medium: Nutrient mixture F12 (DMEM/F12) (Invitrogen) supplemented with 10% foetal bovine serum (Invitrogen), maintained at 37°C, 5% CO^2 and reached the confluency of 60-80% at the day of transfection. The CRISPR transfection was carried out using nucleofection where 1 million cells resuspended in electroporation buffer (90mM Sodium Phosphate, 5mM KCl, 0.15mM CaCl2, 50mM HEPES) were mixed with the RNP complex (2.5µM gRNA, 4mg/ml polyglycolic acid (PGA) and 1.25µM Alt-R® S.p. HiFi Cas9 Nuclease V3 (IDT)), HDR template (IDT, 2µM) and electroporation enhancer (IDT, 1µM). Electroporation was carried out using a 2mm cuvette (VWR) and the G-004 programme on the Nucleofector™ II/2b Device (Lonza). Immediately after electroporation, cells were plated in a 6-well plate in culture medium containing 1µM of HDR enhancer (IDT) for 48 hours before clonal selection and genotyping.

Clonal selection and genotyping

Cells were re-plated in 100 mm dishes at either 1000 or 2500 cells per plate 48 hours after nucleofection and were left to grow into individual colonies which were picked in the next 1-2 weeks. The colonies of cells were then dispersed with trypsin and plated into two identical 96-well plates, one for genotyping and one for further expansion. The cells for genotyping were lysed in lysis buffer (10mM Tris-HCL 7.5pH, 50mM KCl, 1.5mM MgCl2, 0.45% Tween20, 0.5% Triton-X, 20mg/ml Proteinase K). The cell lysates were incubated on the thermocycler for 10 minutes at 56°C to activate the proteinase K followed by 10 minutes at 95°C to stop the enzyme reaction. The crude cell extract was used as template for PCR amplifying fragments containing the CRISPR-edited sites using primers of 5'-GTTAACACAGTATGGATTC-3' and 5'-TATTCAGCATGCACTAAGG-3' to generate a 441bp PCR product to genotype K181E site, and 5'-TCGACTGAAATATCACTGC-3' and 5'-AACCCCACTGTCTACATTCCC-3' to generate a 691bp PCR product to genotype K263E site. PCR was conducted using the VeriFi™ Polymerase reagents (PCR Biosystems) and ran under recommended thermocycler conditions. PCR products were enzymatically cleaned using ExoSAP-IT™ (ThermoFisher) before submission for Sanger Sequencing (Genewiz, Azenta Life Sciences) using the following sequencing primers: K181E forward 5'-AGCCACTGCATCCAGTTGAAACC-3', K181E reverse 5'-TTTCATGAACACACCCTGCCGC-3', K263E forward 5'-CAGTCTCTTTGTGGAGAGG-3' and K263E reverse 5'-TCCCTCTGCATGTTGCCTTG-3'.

RNA extraction and RT-PCR

RNA was extracted using the RNeasy® Mini Kit (Qiagen) with DNase I treatment. cDNA was generated using the SuperScript™ III First-Strand Synthesis Kit (Invitrogen) with 50ng/µL random

hexamer primer (Thermo Fisher). 50ng of cDNA was used for RT-PCR. Primers (Table 1) were designed using Ensembl (https://www.ensembl.org/index.html) and ncbi primer blast (https://www.ncbi.nlm.nih.gov/tools/primer-blast/), unless otherwise stated. All products were run on 2-2.5% agarose gels. The fluorescent tag IRDye 700 was attached to the 5' end of the forward primer of *Poldip3*, the splicing assay of which was visualised by the iBright imaging system (ThermoFisher). All other genes were visualised with standard UV imaging. Bands were quantified by Fiji (21).

RNA-Sequencing

Next-generation RNA sequencing (RNA-Seq) was carried out on three independent RNA extractions per CRISPR clones and wild type (WT) SH-SY5Y cells as control. After RNA extraction, samples with A260/280 reads between 1.8 and 2.1 and RNA integrity numbers (RIN) of 10, determined by nanodrop 2000 (Thermo Fisher) and Agilent 2100 BioAnalyser (Agilent), respectively, were used for library preparation. Libraries were generated from >2µg of total RNA following poly(A) selection by Genewiz (Azenta Life Sciences). Sequencing using NovaSeq 6000 (Illumina) generated 2x150-bp reads at a minimum of 30 million read pairs per sample.

Gene expression profiling

All sequencing reads passed all standard quality metrics as summarised by FastQC v0.12.1 (22). Reads were pseudo-aligned to Gencode v44 transcripts using kallisto v0.48 (23). Gene-level and transcript-level transcript per million (TPMs) were generated from the kallisto abundance files using the R package tximport v1.24.0 (24). Univariate differential expression analysis was performed on the gene-level and transcript-level using sleuth v0.30.0 (25) in R v4.2.1 (26). The thresholds for significance were $q < 0.05$ or 0.1 and absolute log2(fold change) ≥1. Volcano plots were generated on GraphPad Prism version 9.4.1 for Windows. Gene Set Enrichment Analysis (GSEA) was run using the R package fgsea (27) using the prerank setting based on πvalues (-log10(q-value) x log2(fold change)) (28). Enriched sets were identified from the v2023.2 MSigDB gene ontology biological processes and cellular components gene sets (29). Gene ontology information was presented using SRPlot (30). Isoform switching analysis was performed based on the kallisto abundance files using the IsoformSwitchAnalyzeR v1.16.0 (31). The thresholds for significance were $q < 0.05$ and absolute difference in isoform fraction (dIF) ≥0.1.

Antibodies

The antibodies used in this study include mouse beta-III tubulin (1:200, Antibodies.com, A86691), chicken MAP2 (1:5000, Antibodies.com, A85363), rabbit recombinant anti-TDP-43 (1:1000; Proteintech, 80002-1-RR), rabbit cleaved caspase-3 (1:1000; Cell Signalling, 9664S), goat anti-rabbit IgG (H+L) DyLight 488 secondary (1:500, Invitrogen), goat anti-mouse IgG (H+L) DyLight 550 secondary (1:500, Invitrogen), goat anti-rabbit IgG (H+L) DyLight 550 secondary (1:500; Invitrogen) and goat anti-chicken IgY (H+L) Alexa Fluor 650 secondary (1:500, Invitrogen).

SH-SY5Y differentiation

SH-SY5Y cells were plated on collagen-coated (0.05mg/ml, Sigma) plates in standard media (DMEM/F12 +10% FBS) for 24 hours before media was replaced with DMEM + 15% FBS containing 10µM retinoic acid (Sigma, R2625). This media was refreshed every 2 days. At day 5, cells were washed three times with serum free DMEM, before continued culturing in serum free DMEM containing 50ng/ml BDNF (Qkine, Qk050). Medium was refreshed every 2 days and cells harvested or fixed after 4 days in BDNF for further analysis.

Immunofluorescence

Cells were fixed in 4% paraformaldehyde for 30 min and washed with PBS three times for 5 min. Cells were permeabilised by incubation in 0.5% Triton X-100 (Sigma) in PBS for 15 min at room temperature, followed by blocking in 1% goat serum(diluted in PBS) for 1 hour at room temperature. Cells were incubated with primary antibodies diluted in blocking solution overnight at 4°C. After washing in PBS three times for 5 min, cells were subsequently incubated with fluorescent secondary antibodies diluted in the blocking solution for 1 hour at room temperature. DAPI (Sigma) was then used to stain for nuclei before being mounted on coverslips using FluorSave Reagent (Merck).

Neurite growth analysis

Cells stained with MAP2 were imaged on Axio Observer 7 (Zeiss). Neurites from individual cells were traced with NeuronJ plugin on Fiji (32) and quantified for sum neurite length (µm). A minimum of thirty cells were traced across three individual repeats.

Results

Establishment and validation of the CRISPR/Cas9-K181E and K263E knock-in SH-SY5Y cell lines

To investigate disease-causing RNA-binding deficient TDP-43-mediated pathogenesis mechanisms, K181E and K263E mutations were introduced to the *TARDBP* gene in human neuroblastoma cell line SH-SY5Y via CRISPR/Cas9 editing (Figure 1A). From two independent transfections and screening of 110-130 clones per genotype, multiple clones of either homozygous or heterozygous K181E- and K263E-TDP-43 cells were isolated and validated. The nucleotide substitutions were validated by sequencing the genomic DNA of the targeted area and *TARDBP* cDNA (Supplementary Figure 1A). The integrity of *TARDBP* cDNA was also checked, and no chromosome rearrangement or disruption of *TARDBP* gene was observed (Supplementary Figure 1B).

The knock-ins were then functionally validated via examination of the splicing pattern for the most well-known target of TDP-43, *PolDip3* (33), commonly used as a reporter for TDP-43-mediated RNA regulation. Indeed, splicing analysis showed significant reduction of the shorter splicing form of *PolDip3* compared to WT SH-SY5Y cells (Supplementary Figure 1C), consistent with previous reporting that both K181E- and K263E-TDP-43 fail to bind and mediate the exclusion of the cryptic exon 3 of *PolDip3* mRNA (10). Introduction of these disease-linked RNA-binding mutations do not cause prominent nuclear aggregation of TDP-43 protein as seen in the case of overexpression (10), but nuclear speckles of TDP-43 protein distribution are observed compared to the diffuse nuclear TDP-43 in unmodified cells (Figure 1B). Introduction of either K181E or K263E mutations also make cells less viable compared to unmodified cells (Figure 1C).

Overall, we established and validated cell lines using CRISPR/Cas9 to mediate the nucleotide substitution, introducing the disease-causing K181E- or K263E-TDP-43 mutation in either homozygous or heterozygous form where the mutant and wild-type protein is expressed at endogenous level. We validated the cells as disease cell models, observing disrupted splicing patterns of known TDP-43 target mRNA, altered TDP-43 protein distribution and reduced viability.

Differences in K181E-TDP-43 homozygous and heterozygous transcriptomic profiles in comparison to wild-type cells observed by RNA-seq analysis.

To investigate potential cellular dysfunction caused by both K181E and K263E mutations, the transcriptomic profiles of K181E- and K263E-TDP-43 cell lines were established. Bulk RNA-seq was conducted on individual K181E- and K263E-TDP-43 homozygous and heterozygous lines, compared with un-edited SH-SY5Y cells. Using a significance cut-off of $q<0.1$, we found no significant

differential expressed genes (DEGs) between the K263E-TDP-43 cells and control cells (Supplementary Figure 2). When comparing K181E-TDP-43 cells with control, 233 and 167 DEGs were identified in K181E-TDP-43 homozygous and heterozygous cells respectively ($q<0.1$; Figure 2A-B, Supplementary Data 1). Interestingly, the gene expression changes in K181E-TDP-43 heterozygous versus homozygous cells do not follow an incremental pattern of increase or decreased abundance, nor do these changes occur in the expected direction consistent with mutation dosage. As shown in Figure 2C, the DEGs that are up-regulated in K181E-TDP-43 homozygous cells are often seen down-regulated in K181E-TDP-43 heterozygous, and the genes down-regulated in homozygous are seen up-regulated in the heterozygous cells. Further comparison between K181E-TDP-43 homozygous and heterozygous cells identified 997 genes that express at significantly different levels between the two and at a more stringent significance cut-off ($q<0.05$; Figure 2D, Supplementary Data 1), highlighting that homozygous and heterozygous expression of these mutant-TDP-43 have divergent impacts on cells.

As both mutations disrupt a critical, identified function of TDP-43 protein in interrupting its binding to RNA, it has been suggested that they are loss-of-function mutations for TDP-43 (10,18,20). To examine the hypothesis, we compared the transcriptomic data of our CRISPR/Cas9 knock-in cells with the TDP-43 knockdown dataset (14). No obvious patterns of similarities or differences were observed (Supplementary Figure 3A) and only 12 DEGs were shared in both K181E-TDP-43 homozygous and the TDP-43 knockdown (Supplementary Figure 3B). This observation indicates that while K181E-TDP-43 and K263E-TDP-43 are most noticeable for their disruption in TDP-43 binding to its target RNA, their pathological impact cannot be entirely attributed to the simple loss of function of the TDP-43 protein.

Neuronal and synaptic pathways are significantly down-regulated in K181E-TDP-43 homozygous cells.

To investigate the cellular pathways most affected by K181E mutations, gene set enrichment analysis for gene ontology terms was then carried out to assess DEGs identified in the K181E-TDP-43 homozygous and heterozygous comparison. Out of the significant pathways highlighted for DEGs down-regulated in K181E-TDP-43 homozygous cells, approximately a third were neuronally related, including those in the top ten most significant (Figure 3A, Supplementary Data 1). Comparing Log2 fold changes to the average transcripts per million (TPMs) for the DEGs in K181E-TDP-43 homozygous showed that the genes most closely associated with the top pathways involving neuronal or synapse growth (Figure 3A) are those showing the greatest negative fold change (Figure 3B). Other significant pathways down-regulated in K181E-TDP-43 homozygous cells included those related to transport, secretion and general biogenesis and signalling (Figure 3C; Supplementary Data 1), again indicating a potential functional compromise in neurite establishment and neuronal communication. In contrast, the gene ontology term analysis of the up-regulated DEGs in K181E-TDP-43 homozygous cells highlighted more generic pathways and functions such as negative regulation of response to stimulus or cell adhesion (Supplementary Figure 4).

Notably, the most significant genes linked to neuronal and synaptic functional pathways consistently display an opposing expression pattern in K181E-TDP-43 homozygous compared to heterozygous cells, in that the neuron-related genes are down-regulated in K181E-TDP-43 homozygous cells, but up-regulated in K181E-TDP-43 heterozygous cells compared to unmodified cells, whereas the cellular response genes that are up-regulated in K181E-TDP-43 homozygous cells are reduced in K181E-TDP-43 heterozygous cells (Figure 3D). The known TDP-43 targets implicated in ALS disease pathogenesis, STMN2, UNC13A and NPTX2 (13–16,34), also show this similar opposing expression pattern, being down-regulated in K181E-TDP-43 homozygous cells but up-regulated in K181E-TDP-43 heterozygous cells (Figure 3D).

Overall, our data suggest that K181E-TDP-43 expression significantly compromises the transcriptomic profile of the cells, most significantly the genes involved in neuronal and synaptic functions. The direction of the impact appears to depend on whether the mutant TDP-43 is expressed in the homozygous or heterozygous manner.

Transcript isoform switching identified between K181E homozygous and heterozygous cells

Following the investigation of changes to gene levels, we next examined whether the expression of K181E-TDP-43 alters transcript isoform shifts which can occur without an overall gene change (35–37). The isoform switching analysis identified approximately 7000 significant isoform changes for K181E-TDP-43 homozygous cells and around 400 for K181E-TDP-43 heterozygous cells compared to WT cells ($q<0.05$; Figure 4A-B, Supplementary Data 1), indicating that the homozygous expression of K181E-TDP-43 has a stronger influence on alternative splicing compared to the heterozygous expression, despite a similar number of overall differentially expressed genes. Further analysis found that the types of alternative splicing events were induced to similar levels in both homozygous and heterozygous K181E-TDP-43 (Figure 4C).

Comparing K181E-TDP-43 homozygous to K181E-TDP-43 heterozygous led to greater abundance of genes with isoform switches, totalling around 10,000 significant transcript changes ($q<0.05$; Figure 4D, Supplementary Data 1), again highlighting the greatest disparity occurring between the two genotypes. This analysis pulled out a novel set of genes compared to the DEGs identified through whole-gene level analysis (Figure 2). However, when applied to the same gene ontology analysis, these genes are again related to neuronal and synaptic pathways, with an enrichment around cytoskeleton and transport (Figure 4E). One of the most significantly affected genes for both K181E-TDP-43 homozygous comparison to WT, and comparison to K181E-TDP-43 heterozygous was *DCTN1*, which encodes dynactin-1, the largest component of the dynactin complex that has critical roles in axonal and cytoplasmic transport, and cytoskeleton assembly (38). We observed a complete isoform switch in K181E-TDP-43 homozygous from the canonical *DCTN1-228* transcript to *DCTN1-203* (Figure 4F). Using tissue-specific gene expression data acquired from the Genotype-Tissue Expression (GTEx) Portal (https://gtexportal.org/home/), we found that the *DCTN1-228* transcript is highly expressed in several brain regions, while *DCTN1-203* is hardly expressed (Figure 4G). The switch to *DCTN1-203* in the homozygous could contribute functionally to the state of the cells similarly to the overall down-regulation of neuronal genes.

Isoform switching analysis on K263E-TDP-43 homozygous and heterozygous cells in comparison to WT cells identified around 180 and 600 isoform changes respectively (Supplementary Figure 5A-B; Supplementary Data 1) with similar alternative splicing event frequencies (Supplementary Figure 5C).

In summary, isoform switching analysis highlighted transcript dysregulation caused by changes in splicing events due to K181E-TDP-43 expression. Interestingly, the most prominent changes are again attributed to genes involved in neuronal and synaptic pathways, suggesting the main disruption of K181E-TDP-43 expression would be in neuronal health and functions.

Neuronal dysregulation caused by K181E-TDP-43

The RNA-seq results suggest K181E-TDP-43 expression most prominently affects the expression and/or transcript isoforms of genes involved in neuronal growth and synapse development (Figure 3-4). To validate this result, we adapted a published protocol to differentiate SH-SY5Y cells (39) into MAP2 and βIII-tubulin positive neurons with characteristic neurite projections (Figure 5A). First, the differentiation efficiency was examined using MAP2 as markers of mature neurons. As seen in Figure 5B, reduced MAP2 staining was observed in K181E-TDP-43 homozygous, K263E-TDP-43 homozygous and heterozygous cells across differentiation in comparison to WT cells, but not in K181E-TDP-43

heterozygous cells. In fact, K181E-TDP-43 heterozygous cells had increased MAP2 staining at the undifferentiated stage in comparison to WT. Quantification of MAP2 mRNA via RT-PCR also confirmed this observation that MAP2 was mostly reduced in expression at all stages of differentiation in mutant cells except for K181E-TDP-43 heterozygous cells (Figure 5C). This is consistent with the earlier observation in the RNA-seq study that the neuronal-linked genes are down-regulated in K181E-TDP-43 homozygous cells but up-regulated in K181E-TDP-43 heterozygous cells (Figure 3D). From the cells that were positive for MAP2 (Figure 5B), the sum neurite lengths of individual cells were subsequently quantified (Figure 5D). As shown in figure 5D, the neurite lengths of the MAP2-positive differentiated cells were reduced in K181E-TDP-43 homozygous cells. However, K181E-TDP-43 heterozygous cells exhibited longer neurites compared to control in undifferentiated condition and similar neurite length to control when differentiated (Figure 5D). Examination of the neuronal-linked genes identified in the RNA-seq confirmed that they were down-regulated in K181E-TDP-43 homozygous cells but up-regulated in K181E-TDP-43 heterozygous cells in the undifferentiated condition (Figure 5E; Supplementary Figure 6A) which could be the reason why K181E-TDP-43 homozygous cells cannot differentiate efficiently and why K181E-TDP-43 heterozygous cells appear to be primed with MAP2 induction and longer neurites even in the undifferentiated condition (Figure 5B-D). The gene expression after differentiation showed a similar pattern, that neuronal-linked genes were still reduced in K181E-TDP-43 homozygous cells (Figure 5E; Supplementary Figure 6B). Their levels in K181E-TDP-43 heterozygous cells were mostly similar to WT, however, some neuronal genes exhibited decreased expression in a similar manner to K181E-TDP-43 homozygous cells, including *PTPRN2*, *GRIN1* and *SLIT1* (Figure 5E; Supplementary Figure 6B). Since K181E-TDP-43 heterozygous differentiated cells displayed similar neurite growth and overall morphology as WT cells once differentiation was initiated, potentially the genes that begin to align with the homozygous state are less vital for these processes to occur.

The examination of selected genes seen up-regulated in K181E-TDP-43 homozygous cells also verified the earlier results from RNA-seq, in that the up-regulation in K181E-TDP-43 homozygous cells and down-regulation in K181E-TDP-43 heterozygous cells was validated in the RT-PCR (Figure 5E; Supplementary Figure 6C). This pattern was largely maintained in differentiated cells except for *S100A11* and *COL3A1* whose expression level seem to even out in all genotypes in differentiated cells (Figure 5E; Supplementary Figure 6D). Finally, the expression levels of the known TDP-43 targets, *STMN2* and *UNC13A*, were also validated in these cells in both undifferentiated and differentiated conditions. A more significant difference was observed between K181E-TDP-43 homozygous and WT cells after differentiation (Figure 5E; Supplementary Figure 6E-F), highlighting them as more mature neuron TDP-43 targets. K181E-TDP-43 heterozygous cells began to see a reduction in *UNC13A* after differentiation, but not in *STMN2* (Figure 5E; Supplementary Figure 6F).

The K263E mutation affects RRM2 which is proposed to play a minor role in binding to TDP-43's target RNA (5,40) especially when the mutant protein is expressed at endogenous levels. Whereas no prominent transcriptomic profile change was observed using undifferentiated K263E-TDP-43 homozygous and heterozygous cells, they did begin to exhibit some deficits once differentiation begins (Figure 5B-D) with the neuronal-linked genes down-regulated in a similar manner to K181E-TDP-43 homozygous, alongside known targets *STMN2* and *UNC13A* (Figure 5E; Supplementary Figure 6). All functional observations were confirmed in independent lines for K181E-TDP-43 heterozygous and K263E-TDP-43 homozygous and heterozygous (Supplementary Figure 7).

Discussion

TDP-43 pathology is a contributing factor to ~95% of ALS and ~50% of FTD (1), and is also strongly associated with severe AD (2,3). Characterisation of the cause-and-effect underlying TDP-43 proteinopathy is therefore a necessary key in unravelling the disease, and to develop targeted therapy. In this study, we developed CRISPR/Cas9 knock-ins of two ALS/FTD-associated RNA-binding

deficient TDP-43 mutants, K181E and K263E, into human neuroblastoma SH-SY5Y cells, creating homozygous and heterozygous K181E- and K263E-TDP-43 cell lines that cause splicing changes of known TDP-43 targets such as *Poldip3* (Supplementary Figure 1) (33) and exhibit lower cell viability (Figure 1C). Further transcriptomic analysis identified significant changes in K181E-TDP-43 cells, particularly highlighting decreases in expression of genes involved in neuronal and synaptic development, organisation and signalling (Figure 3-4). The functional impact of this transcriptional dysregulation was validated in cell studies where the disruption in neuronal differentiation and neurite growth was observed in all TDP-43 mutant cells except for K181E-TDP-43 heterozygous cells which show hints of being primed for neuronal differentiation even in basal condition (Figure 5).

RNA-binding proteins (RBPs) in Neurodegeneration

There are well over 1000 RBPs in either the nucleus or the cytoplasm regulating mRNA stability, transport and maturation (41,42). Typically, these proteins contain RNA recognition motifs (RRMs), nuclear import and export signals, and aggregation-prone low complexity domains (LCDs) (43–45). They can form RNA-protein (RNP) granules that can have different roles depending on contributing factors (46–49).

RNA regulation and RBPs play pivotal roles in neuronal health and maintenance (50–52). Some RBPs are only specifically localised to neurons (52), and it has been shown that the brain, as a whole, undergoes increased levels of alternative splicing compared to other tissues in a tightly regulated manner (53,54). Over time, more classes of RNAs that interact with RBPs have been identified that contribute to refining gene expression in brain cells allowing for the neuronal specific proteome and adaptive nature (55–58). In addition, RPBs are also instrumental for local translation taking place in neuronal axons, dendrites and synaptic boutons (59,60).

The importance of RBPs to neurons is most strikingly shown through their frequent genetic and pathological associations with neurological diseases. For example, mutations to the pre-mRNA alternative splicer RBFOX3 have been linked to cognitive impairment, autism and neurodevelopmental delays, while several members of the ELAVL family of RBPs are found to contribute to neurodevelopmental defects (61–63). Notably, in neurodegenerative diseases, TDP-43, FUS, TIA1, hnRNPA2B1 and hnRNPA1 are pathological drivers of familial and sporadic ALS and FTD, hnRNP A1 is associated with multiple sclerosis (MS), and Tau RNA-binding dysregulation has been implicated in AD and FTD (1,64–70).

The aggregation-prone LCD of RBPs has the potential to prompt the formation of hallmark proteinopathies linked to neurodegenerative diseases (8,9,64,71,72). In normal conditions, the LCD is involved in the formation of RNPs through liquid-liquid phase separation (LLPS), a biochemical process that forms dynamic non-membrane bound complexes in the cytoplasm that can enable RNA transport and interaction (Lin et al., 2015; Molliex et al., 2015)(Lin et al., 2015; Molliex et al., 2015)(Lin et al., 2015; Molliex et al., 2015)(Lin et al., 2015; Molliex et al., 2015)(Lin et al., 2015; Molliex et al., 2015)(Lin et al., 2015; Molliex et al., 2015). Disease-linked mutations in the LCD have been shown to increase the propensity of protein aggregation during LLPS, potentially prompting the mis-folding and aggregated protein pathology, particularly in ALS (75,76). In a similar vein, RRMs are also shown to contribute to RBP aggregation. TDP-43 RRM1 and FUS RRM were observed to self-assemble to form fibril-like aggregates, and TDP-43 RRMs have been found repeatedly in the aggregates of ALS brains (77,78). Disruption in RBPs subsequently leads to a cascading effect that further compromises neuronal health. One of the most evident impacts is RNA splicing dysregulation which is an established contributing factor to neurodegenerative diseases (79). For example, TDP-43 loss-of-function and disease-relevant TDP-43 mutation models have been seen to contribute to

widespread splicing changes that would contribute to neurodegenerative phenotypes (4,14,16,20,35,80). Similar mis-splicing can also be seen in spinal muscular atrophy (SMA), where whole splicing machinery complexes are affected, and in Alzheimer's Disease, where components of the spliceosome accumulates within aggregates contributes to mis-splicing and downregulation of GABAergic synaptic genes (81–84). While these splicing deficits can occur as a consequence of aggregates recruiting RBPs precipitating their loss of function, there is evidence suggesting that these events may be occurring ahead of aggregation due to mislocalisation of the protein or other cellular factors (81,85–88).

TDP-43 RNA-Binding Deficiency and Disease Development

TDP-43 is a prominent RBP associated with neurodegenerative diseases, associated with ~97% of ALS cases, ~50% FTD cases, and severe cases of Alzheimer's (1,3,18,86). TDP-43 is ubiquitously expressed, and knock-outs in mice lead to embryonic lethality (89). Overexpression models are also seen to cause cytotoxicity, meaning regulated TDP-43 levels are vital in maintaining cell health (34,90,91).

Despite the close association between TDP-43 proteinopathy and ALS/FTD, the involvement of TDP-mediated RNA regulation had been overlooked for a long time due to the hot spots of disease-linked TDP-43 mutations concentrated in the C-terminal LCD of the protein, away from the RRMs (11). *In vitro* studies have found that the C-terminal mutations such as Q331K and M337V do not interfere with TDP-43 binding to its target RNA (10), and that the expression of the engineered RNA-binding deficient F147/149L-TDP-43 does not cause any further deficiency in cell function or survival (92,93).The question remains: to what extent is RNA-binding disruption an integrated mechanism of TDP-43 disease-driving?

In 2009 and 2019, the two TDP-43 RNA-binding deficient mutations, K181E and K263E, were identified in independent families of ALS and FTD (10,18). Both mutations cause hyperphosphorylated and insoluble nuclear TDP-43 aggregates in both patient tissue and through overexpression models (10,18), and unlike with the artificial F147/149L-TDP-43, these ALS/FTD-linked mutations lead to cellular disruption and cytotoxicity. As shown in this study, despite no overt nuclear aggregates besides infrequent nuclear speckling observed when the mutant protein was expressed at the endogenous level (Figure 1B), due to either the lack of challenge, or the endogenous expression being insufficient to drive aggregation formation, the introduction of these mutations does lead to global transcriptomic changes in gene expression (Figure 2-4) and affect cell survival and function (Figure 1C, 5).

While K181E- and K263E-TDP-43 were observed to have similar affects in the *PolDip3* splicing assay (Supplementary Figure 1C), this was not extended to the RNA-sequencing results themselves. K263E-TDP-43 showed no differentially expressed genes when compared to unmodified SH-SY5Y cells in their undifferentiated state (Supplementary Figure 2). This is somewhat unsurprising as Imaizumi et al. (20) have previously reported no differences in K263E-TDP-43 homozygous knock-in in undifferentiated iPSCs. Once differentiated, we did observe some significant changes to gene expression through RT-PCR and consequential effects on neuronal health, including a down-regulation of *STMN2* and *UNC13A* (Figure 5; Supplementary Figure 6), consistent with published K263E models and broader knockdown models (13–16,20). On the other hand, K181E-TDP-43 homozygous and heterozygous cells did show significant changes in transcriptomic profile in comparison to the WT cells (Figure 2). Unlike the K263E adjacent RRM2 which is suggested to play a supporting role in facilitating RRM1-RNA binding (94), K181E is found adjacent to RRM1 which is readily associated to TDP-43's autoregulation, managing its levels in the nucleus (94,95), and has

been associated with TDP-43's ability to undergo liquid-liquid phase separation during cellular stress (96).

In general, ALS and FTD are age-related diseases where aberrant proteins and harmful substances accumulate over time. Whereas wild-type or LCD mutant TDP-43 can still bind to target RNA, overexpression leads to splicing misregulation, similar to observations in TDP-43 knock-down (10,35,37,97). This is likely due to the changes in the pool of functional TDP-43 via its nuclear clearance and increased aggregation, lending support to the theory that TDP-43 loss-of-function is a driver of pathology. This is further supported by knock-down studies which identified around 100 cryptic exon-containing transcripts which are the targets of nonsense-mediated decay (NMD) and other degradation pathways (98), leading to protein down-regulation. Two prominent ALS-linked targets of TDP-43 are *STMN2* and *UNC13A*. Under TDP-43 depletion, the full-length *STMN2* decreased while the truncated *STMN2* increased through cryptic exon inclusion, leading to deteriorated motor neuron health (14,15,17). *UNC13A* is a critical gene for synapse function, with SNPs near to the cryptic exon of *UNC13A* seen to upregulate cryptic splicing and alter the ability of TDP-43 to bind and repress the cryptic exon inclusion. The resulting transcript is degraded by NMD, decreasing the overall level of the functional protein (13,16). The changes of TDP-43 targets such as *STMN2* and *UNC13A* are also seen in ALS and FTD patient tissues (13–16), and the overexpression of full-length *STMN2* and use of antisense oligonucleotides to rectify *UNC13A* cryptic exon inclusion rescue toxicity in ALS cell models (14,99–101), suggesting that disruption of TDP-43-mediated RNA regulation is indeed a contributing factor for ALS development. Furthermore, high levels of cryptic exon inclusion have also been identified in AD, with *STMN2* and *UNC13A* cryptic exons detected in TDP-43-associated AD (102,103), again, highlighting the role of TDP-43-mediated RNA regulation in neuronal health and the importance in getting a better understanding of its impact. However, it should be noted that the loss-of-function cannot be the sole cause of TDP-43-mediated pathogenesis as no cellular toxicity is seen by the expression of non-disease-linked RNA-binding deficient F147/149L-TDP-43. The dysregulation of RNA-regulation is likely an aggravating factor that jointly with TDP-43 gain-of-toxicity triggers disease development and progression.

Dosage-dependent opposing effect of K181E-TDP-43

Most interestingly from the RNA-seq data is that the greatest difference in gene expression occurred between the two K181E-TDP-43 genotypes, where we see the DEG changes in opposite directions in the homozygous and heterozygous K181E-TDP-43 cells, either sides of the unmodified wild-type (Figure 2). The genes that are down-regulated in the homozygous and up-regulated in the heterozygous were significantly associated with neuronal and synaptic processes (Figure 3). This feature is observed at both overall gene level (Figure 2) and also on the level of transcript isoform shift (Figure 4).

The down-regulation of these genes or the shift to non-neuronal isoforms in K181E-TDP-43 homozygous cells compromises neuronal differentiation, while opposing expression of these genes in K181E-TDP-43 heterozygous cells appear to prime them for neuronal differentiation in the absence of stimulating factors (Figure 5). This could imply a compensatory mechanism occurring to protect neuronal growth at the detriment to other processes, since these cells exhibit similar cytotoxicity as the other genotypes (Figure 1C). Overproduction of neurons, dendritic overgrowth and excess synaptic connections have been associated to neurodevelopmental disorders such as autism spectrum disorders (ASD) (104–106), and also with neurodegenerative diseases. A recent study by Capizzi et al. (107) observed that whereas axons from Huntington Disease (HD) mouse model brains were shorter and less able to cross the corpus callosum to the other hemisphere, the axons that were able to cross, had increased dendritic branching, hypothesised by the researchers to

be a compensatory action in response to the lower number of surviving neurons. In Parkinson's Disease (PD), increased neuronal connectivity as a result of PD-related genetic mutations were correlated to severity and aggressiveness of the disease in patients (108). And in ALS, neurite overgrowth and enlarged axonal arbors to compensate the loss of NMJ innervation was observed in mouse models (109,110). This again signifies a balance between pathogenic and compensatory mechanisms in development, with disease-associated factors even at times playing a protective role in early life. The link between neurodevelopmental and neurodegenerative disorders is a tenuous one. In terms of ALS and FTD, several studies have shown their correlation and co-morbidity to neurodevelopmental and psychiatric disorders, often related to psychological and physical hyperactivity (111–113). Cellular stressors have been linked to these neurodevelopmental disorders (114–116), but how this may or may not develop into neurodegenerative diseases is not understood.

Overall, our study demonstrated the impact on transcriptomic profiles by disease-linked TDP-43 RNA-binding deficiency. The most affected pathways are related to neuronal development, synaptic processes and cellular transport, and as such, had functional consequences on the cells differentiation and survival. K181E-TDP-43 heterozygous expression appeared to aggravate cellular disturbance in an opposite direction to homozygous K181E-TDP-43 cells. The extent of the disruption correlating to ageing and subsequent challenges still needs to be further investigated, but could potentially shed light on the early-stage pathogenesis for disease.

Data Availability

RNA-Sequencing data for all genotypes is now available following the SRA accession number: PRJNA1191337.

Funding Sources

This work was supported by the Academy of Medical Science (AMS, with Wellcome Trust, BEIS, the British Heart Foundation and Diabetes UK) [SBF006\1088] to HJC; and the Biology departmental PhD studentship to MM. RTG and ASM were supported by ASM's York Against Cancer (York, UK) 30th Anniversary Lectureship in Cancer Informatics.

References

1. Neumann, M., Sampathu, D.M., Kwong, L.K., Truax, A.C., Micsenyi, M.C., Chou, T.T., Bruce, J., Schuck, T., Grossman, M., Clark, C.M., *et al.* (2006) Ubiquitinated TDP-43 in Frontotemporal Lobar Degeneration and Amyotrophic Lateral Sclerosis. *Science (1979)*, **314**, 130–133.

2. Amador-Ortiz, C., Lin, W.L., Ahmed, Z., Personett, D., Davies, P., Duara, R., Graff-Radford, N.R., Hutton, M.L. and Dickson, D.W. (2007) TDP-43 immunoreactivity in hippocampal sclerosis and Alzheimer's disease. *Ann Neurol*, **61**, 435–445.

3. Uryu, K., Nakashima-Yasuda, H., Forman, M.S., Kwong, L.K., Clark, C.M., Grossman, M., Miller, B.L., Kretzschmar, H.A., M-Y Lee, V., Trojanowski, J.Q., *et al.* (2008) Concomitant TAR-DNA-Binding Protein 43 Pathology Is Present in Alzheimer Disease and Corticobasal Degeneration but Not in Other Tauopathies. *J Neuropathol Exp Neurol*, **67**, 555–564.

4. Tollervey, J.R., Curk, T., Rogelj, B., Briese, M., Cereda, M., Kayikci, M., König, J., Hortobágyi, T., Nishimura, A.L., Župunski, V., *et al.* (2011) Characterizing the RNA targets and position-dependent splicing regulation by TDP-43. *Nat Neurosci*, **14**, 452–458.

5. Buratti, E. and Baralle, F.E. (2001) Characterization and Functional Implications of the RNA Binding Properties of Nuclear Factor TDP-43, a Novel Splicing Regulator of CFTR Exon 9. *Journal of Biological Chemistry*, **276**, 36337–36343.

6. Arai, T., Hasegawa, M., Akiyama, H., Ikeda, K., Nonaka, T., Mori, H., Mann, D., Tsuchiya, K., Yoshida, M., Hashizume, Y., *et al.* (2006) TDP-43 is a component of ubiquitin-positive tau-negative inclusions in frontotemporal lobar degeneration and amyotrophic lateral sclerosis. *Biochem Biophys Res Commun*, **351**, 602–611.

7. Winton, M.J., Igaz, L.M., Wong, M.M., Kwong, L.K., Trojanowski, J.Q. and Lee, V.M.Y. (2008) Disturbance of nuclear and cytoplasmic TAR DNA-binding protein (TDP-43) induces disease-like redistribution, sequestration, and aggregate formation. *Journal of Biological Chemistry*, **283**, 13302–13309.

8. Zhang, Y.-J., Xu, Y.-F., Cook, C., Gendron, T.F., Roettges, P., Link, C.D., Lin, W.-L., Tong, J., Castanedes-Casey, M., Ash, P., *et al.* (2009) Aberrant cleavage of TDP-43 enhances aggregation and cellular toxicity. *PNAS*, **106**, 7607–7612.

9. Yang, C., Tan, W., Whittle, C., Qiu, L., Cao, L., Akbarian, S. and Xu, Z. (2010) The C-terminal TDP-43 fragments have a high aggregation propensity and harm neurons by a dominant-negative mechanism. *PLoS One*, **5**, e15878.

10. Chen, H.J., Topp, S.D., Hui, H.S., Zacco, E., Katarya, M., McLoughlin, C., King, A., Smith, B.N., Troakes, C., Pastore, A., *et al.* (2019) RRM adjacent TARDBP mutations disrupt RNA binding and enhance TDP-43 proteinopathy. *Brain*, **142**, 3753–3770.

11. Pesiridis, G.S., Lee, V.M.Y. and Trojanowski, J.Q. (2009) Mutations in TDP-43 link glycine-rich domain functions to amyotrophic lateral sclerosis. *Hum Mol Genet*, **18**, 156–162.

12. Sephton, C.F., Cenik, C., Kucukural, A., Dammer, E.B., Cenik, B., Han, Y.H., Dewey, C.M., Roth, F.P., Herz, J., Peng, J., *et al.* (2011) Identification of neuronal RNA targets of TDP-43-containing ribonucleoprotein complexes. *Journal of Biological Chemistry*, **286**, 1204–1215.

13. Brown, A.L., Wilkins, O.G., Keuss, M.J., Hill, S.E., Zanovello, M., Lee, W.C., Bampton, A., Lee, F.C.Y., Masino, L., Qi, Y.A., *et al.* (2022) TDP-43 loss and ALS-risk SNPs drive mis-splicing and depletion of UNC13A. *Nature*, **603**, 131–137.

14. Melamed, Z., López-Erauskin, J., Baughn, M.W., Zhang, O., Drenner, K., Sun, Y., Freyermuth, F., McMahon, M.A., Beccari, M.S., Artates, J.W., *et al.* (2019) Premature polyadenylation-mediated loss of stathmin-2 is a hallmark of TDP-43-dependent neurodegeneration. *Nat Neurosci*, **22**, 180–190.

15. Klim, J.R., Williams, L.A., Limone, F., Guerra San Juan, I., Davis-Dusenbery, B.N., Mordes, D.A., Burberry, A., Steinbaugh, M.J., Gamage, K.K., Kirchner, R., *et al.* (2019) ALS-implicated protein TDP-43 sustains levels of STMN2, a mediator of motor neuron growth and repair. *Nat Neurosci*, **22**, 167–179.

16. Ma, X.R., Prudencio, M., Koike, Y., Vatsavayai, S.C., Kim, G., Harbinski, F., Briner, A., Rodriguez, C.M., Guo, C., Akiyama, T., *et al.* (2022) TDP-43 represses cryptic exon inclusion in the FTD–ALS gene UNC13A. *Nature*, **603**, 124–130.

17. Prudencio, M., Humphrey, J., Pickles, S., Brown, A.L., Hill, S.E., Kachergus, J.M., Shi, J., Heckman, M.G., Spiegel, M.R., Cook, C., *et al.* (2020) Truncated stathmin-2 is a marker of TDP-43 pathology in frontotemporal dementia. *Journal of Clinical Investigation*, **130**, 6080–6092.

18. Kovacs, G., Murrell, J., Horvath, S., Haraszti, L., Majtenyi, K., Molnar, M., Budka, H., Ghetti, B. and Spina, S. (2009) TARDBP variation associated with frontotemporal dementia, supranuclear gaze palsy, and chorea. *Movement Disorders*, **24**, 1842–1847.

19. Yu, H., Lu, S., Gasior, K., Singh, D., Vazquez-Sanchez, S., Tapia, O., Toprani, D., Beccari, M.S., Yates, J.R., Da Cruz, S., *et al.* (2021) HSP70 chaperones RNA-free TDP-43 into anisotropic intranuclear liquid spherical shells. *Science (1979)*, **371**, 1–15.

20. Imaizumi, K., Ideno, H., Sato, T., Morimoto, S. and Okano, H. (2022) Pathogenic Mutation of TDP-43 Impairs RNA Processing in a Cell Type-Specific Manner: Implications for the Pathogenesis of ALS/FTLD. *eNeuro*, **9**, 1–12.

21. Schindelin, J., Arganda-Carreras, I., Frise, E., Kaynig, V., Longair, M., Pietzsch, T., Preibisch, S., Rueden, C., Saalfeld, S., Schmid, B., *et al.* (2012) Fiji: An open-source platform for biological-image analysis. *Nat Methods*, **9**, 676–682.

22. Andrews, S. (2019) FastQC: A quality control tool for high throughput sequence data. FastQC: A quality control tool for high throughput sequence data.

23. Bray, N.L., Pimentel, H., Melsted, P. and Pachter, L. (2016) Near-optimal probabilistic RNA-seq quantification. *Nat Biotechnol*, **34**, 525–527.

24. Soneson, C., Love, M.I. and Robinson, M.D. (2015) Differential analyses for RNA-seq: transcript-level estimates improve gene-level inferences. *F1000Res*, **4**, 1521.

25. Pimentel, H., Bray, N.L., Puente, S., Melsted, P. and Pachter, L. (2017) Differential analysis of RNA-seq incorporating quantification uncertainty. *Nat Methods*, **14**, 687–690.

26. R Core Team (2022) R: A language and environment for statistical computing. R: A language and environment for statistical computing. **(2022)** .

27. Korotkevich, G., Sukhov, V., Budin, N., Shpak, B., Artyomov, M.N. and Sergushichev, A. (2016) Fast gene set enrichment analysis. *bioRxiv*.

28. Xiao, Y., Hsiao, T.H., Suresh, U., Chen, H.I.H., Wu, X., Wolf, S.E. and Chen, Y. (2014) A novel significance score for gene selection and ranking. *Bioinformatics*, **30**, 801–807.

29. Subramanian, A., Tamayo, P., Mootha, V.K., Mukherjee, S., Ebert, B.L., Gillette, M.A., Paulovich, A., Pomeroy, S.L., Golub, T.R., Lander, E.S., *et al.* (2005) Gene set enrichment analysis: A knowledge-based approach for interpreting genome-wide expression profiles. *PNAS*, **102**, 15545–15550.

30. Tang, D., Chen, M., Huang, X., Zhang, G., Zeng, L., Zhang, G., Wu, S. and Wang, Y. (2023) SRplot: A free online platform for data visualization and graphing. *PLoS One*, **18**, e0294236.

31. Vitting-Seerup, K., Sandelin, A. and Berger, B. (2019) IsoformSwitchAnalyzeR: Analysis of changes in genome-wide patterns of alternative splicing and its functional consequences. *Bioinformatics*, **35**, 4469–4471.

32. Meijering, E., Jacob, M., Sarria, J.-C.F., Steiner, P., Hirling, H. and Unser, M. (2004) Design and Validation of a Tool for Neurite Tracing and Analysis in Fluorescence Microscopy Images. *Cytometry*, **58**, 167–176.

33. Shiga, A., Ishihara, T., Miyashita, A., Kuwabara, M., Kato, T., Watanabe, N., Yamahira, A., Kondo, C., Yokoseki, A., Takahashi, M., *et al.* (2012) Alteration of POLDIP3 splicing associated with loss of function of TDP-43 in tissues affected with ALS. *PLoS One*, **7**, e43120.

34. Hruska-Plochan, M., Wiersma, V.I., Betz, K.M., Mallona, I., Ronchi, S., Maniecka, Z., Hock, E.M., Tantardini, E., Laferriere, F., Sahadevan, S., *et al.* (2024) A model of human neural networks reveals NPTX2 pathology in ALS and FTLD. *Nature*, **626**, 1073–1083.

35. Arnold, E.S., Ling, S.C., Huelga, S.C., Lagier-Tourenne, C., Polymenidou, M., Ditsworth, D., Kordasiewicz, H.B., McAlonis-Downes, M., Platoshyn, O., Parone, P.A., *et al.* (2013) ALS-linked TDP-43 mutations produce aberrant RNA splicing and adult-onset motor neuron disease without aggregation or loss of nuclear TDP-43. *PNAS*, **110**, 736–745.

36. De Conti, L., Akinyi, M. V., Mendoza-Maldonado, R., Romano, M., Baralle, M. and Buratti, E. (2015) TDP-43 affects splicing profiles and isoform production of genes involved in the apoptotic and mitotic cellular pathways. *Nucleic Acids Res*, **43**, 8990–9005.

37. Fratta, P., Sivakumar, P., Humphrey, J., Lo, K., Ricketts, T., Oliveira, H., Brito-Armas, J.M., Kalmar, B., Ule, A., Yu, Y., *et al.* (2018) Mice with endogenous TDP -43 mutations exhibit gain of splicing function and characteristics of amyotrophic lateral sclerosis . *EMBO J*, **37**, e98684.

38. Borg, R., Herrera, P., Purkiss, A., Cacciottolo, R. and Cauchi, R.J. (2023) Reduced levels of ALS gene DCTN1 induce motor defects in Drosophila. *Front Neurosci*, **17**, 1164251.

39. Encinas, M., Iglesias, M., Liu, Y., Wang, H., Muhaisen, A., Ceña, V., Gallego, C. and Comella, J.X. (2000) Sequential treatment of SH-SY5Y cells with retinoic acid and brain-

derived neurotrophic factor gives rise to fully differentiated, neurotrophic factor-dependent, human neuron-like cells. *J Neurochem*, **75**, 991–1003.

40. Zacco, E., Martin, S.R., Thorogate, R. and Pastore, A. (2018) The RNA-Recognition Motifs of TAR DNA-Binding Protein 43 May Play a Role in the Aberrant Self-Assembly of the Protein. *Front Mol Neurosci*, **11**.

41. Gerstberger, S., Hafner, M. and Tuschl, T. (2014) A census of human RNA-binding proteins. *Nat Rev Genet*, **15**, 829–845.

42. Gebauer, F., Schwarzl, T., Valcárcel, J. and Hentze, M.W. (2021) RNA-binding proteins in human genetic disease. *Nat Rev Genet*, **22**, 185–198.

43. Lunde, B.M., Moore, C. and Varani, G. (2007) RNA-binding proteins: Modular design for efficient function. *Nat Rev Mol Cell Biol*, **8**, 479–490.

44. Li, Y.R., King, O.D., Shorter, J. and Gitler, A.D. (2013) Stress granules as crucibles of ALS pathogenesis. *Journal of Cell Biology*, **201**, 361–372.

45. King, O.D., Gitler, A.D. and Shorter, J. (2012) The tip of the iceberg: RNA-binding proteins with prion-like domains in neurodegenerative disease. *Brain Res*, **1462**, 61–80.

46. Kedersha, N., Stoecklin, G., Ayodele, M., Yacono, P., Lykke-Andersen, J., Fitzler, M.J., Scheuner, D., Kaufman, R.J., Golan, D.E. and Anderson, P. (2005) Stress granules and processing bodies are dynamically linked sites of mRNP remodeling. *Journal of Cell Biology*, **169**, 871–884.

47. Krichevsky, A.M. and Kosik, K.S. (2001) Neuronal RNA Granules: A Link between RNA Localization and Stimulation-Dependent Translation plastic changes dependent upon synthesis of new pro-teins are probably regulated by local translational con-trol over existing local mRNAs. *Neuron*, **32**, 683–696.

48. Morimoto, R.I. (2011) The heat shock response: Systems biology of proteotoxic stress in aging and disease. *Cold Spring Harb Symp Quant Biol*, **76**, 91–99.

49. Zeitelhofer, M., Karra, D., Macchi, P., Tolino, M., Thomas, S., Schwarz, M., Kiebler, M. and Dahm, R. (2008) Dynamic interaction between P-bodies and transport ribonucleoprotein particles in dendrites of mature hippocampal neurons. *Journal of Neuroscience*, **28**, 7555–7562.

50. Agnes, F. and Perron, M. (2004) RNA-binding proteins and neural development: a matter of targets and complexes. *Neuro Report*, **15**, 2567–2570.

51. Zhou, H.L., Mangelsdorf, M., Liu, J.H., Zhu, L. and Wu, J.Y. (2014) RNA-binding proteins in neurological diseases. *Sci China Life Sci*, **57**, 432–444.

52. De Conti, L., Baralle, M. and Buratti, E. (2017) Neurodegeneration and RNA-binding proteins. *Wiley Interdiscip Rev RNA*, **8**, e1394.

53. Alfonso-Gonzalez, C., Legnini, I., Holec, S., Arrigoni, L., Ozbulut, H.C., Mateos, F., Koppstein, D., Rybak-Wolf, A., Bönisch, U., Rajewsky, N., *et al.* (2023) Sites of transcription initiation drive mRNA isoform selection. *Cell*, **186**, 2438-2455.e22.

54. Yeo, G., Holste, D., Kreiman, G. and Burge, C.B. (2004) Variation in alternative splicing across human tissues. *Genome Biol*, **5**, 74.

55. Wu, P., Zuo, X., Deng, H., Liu, X., Liu, L. and Ji, A. (2013) Roles of long noncoding RNAs in brain development, functional diversification and neurodegenerative diseases. *Brain Res Bull*, **97**, 69–80.

56. Kim, T.K., Hemberg, M., Gray, J.M., Costa, A.M., Bear, D.M., Wu, J., Harmin, D.A., Laptewicz, M., Barbara-Haley, K., Kuersten, S., *et al.* (2010) Widespread transcription at neuronal activity-regulated enhancers. *Nature*, **465**, 182–187.

57. Sauvageau, M., Goff, L.A., Lodato, S., Bonev, B., Groff, A.F., Gerhardinger, C., Sanchez-Gomez, D.B., Hacisuleyman, E., Li, E., Spence, M., *et al.* (2013) Multiple knockout mouse models reveal lincRNAs are required for life and brain development. *Elife*, **2**, e01749.

58. Wang, W., Kwon, E.J. and Tsai, L.H. (2012) MicroRNAs in learning, memory, and neurological diseases. *Learning and Memory*, **19**, 359–368.

59. Jung, H., Yoon, B.C. and Holt, C.E. (2012) Axonal mRNA localization and local protein synthesis in nervous system assembly, maintenance and repair. Axonal mRNA localization and local protein synthesis in nervous system assembly, maintenance and repair. *Nat Rev Neurosci* **(2012)** , *13*, 308–324.

60. Broix, L., Turchetto, S. and Nguyen, L. (2021) Coordination between Transport and Local Translation in Neurons. Coordination between Transport and Local Translation in Neurons. *Trends Cell Biol* **(2021)** , *31*, 372–386.

61. Kim, K.K., Nam, J., Mukouyama, Y.S. and Kawamoto, S. (2013) Rbfox3-regulated alternative splicing of Numb promotes neuronal differentiation during development. *Journal of Cell Biology*, **200**, 443–458.

62. Wang, H.Y., Hsieh, P.F., Huang, D.F., Chin, P.S., Chou, C.H., Tung, C.C., Chen, S.Y., Lee, L.J., Gau, S.S.F. and Huang, H.S. (2015) RBFOX3/NeuN is Required for Hippocampal Circuit Balance and Function. *Sci Rep*, **5**.

63. Mulligan, M.R. and Bicknell, L.S. (2023) The molecular genetics of nELAVL in brain development and disease. *European Journal of Human Genetics*, **31**, 1209–1217.

64. Ticozzi, N., Silani, V., Leclerc, A.L., Keagle, B.P., Gellera, B.C., Ratti, A., Taroni, F., Kwiatkowski, T.J., Mckenna-Yasek, D.M., Sapp, P.C., *et al.* (2009) Analysis of FUS gene mutation in familial amyotrophic lateral sclerosis within an Italian cohort From the Department of Neurology (N. *Neurology*, **9**, 1180–1185.

65. Libner, C.D., Salapa, H.E., Hutchinson, C., Stang, T.E., Thibault, P.A., Hammond, S.A. and Levin, M.C. (2022) Autoimmunity to a ribonucleoprotein drives neuron loss in multiple sclerosis models. *Neurobiol Dis*, **170**.

66. Mackenzie, I.R., Nicholson, A.M., Sarkar, M., Messing, J., Purice, M.D., Pottier, C., Annu, K., Baker, M., Perkerson, R.B., Kurti, A., *et al.* (2017) TIA1 Mutations in Amyotrophic Lateral Sclerosis and Frontotemporal Dementia Promote Phase Separation and Alter Stress Granule Dynamics. *Neuron*, **95**, 808-816.e9.

67. Kim, H.J., Kim, N.C., Wang, Y.D., Scarborough, E.A., Moore, J., Diaz, Z., MacLea, K.S., Freibaum, B., Li, S., Molliex, A., *et al.* (2013) Mutations in prion-like domains in

hnRNPA2B1 and hnRNPA1 cause multisystem proteinopathy and ALS. *Nature*, **495**, 467–473.

68. Lester, E. and Parker, R. (2024) Tau, RNA, and RNA-Binding Proteins: Complex Interactions in Health and Neurodegenerative Diseases. *Neuroscientist*, **30**, 458–472.

69. Kavanagh, T., Halder, A. and Drummond, E. (2022) Tau interactome and RNA binding proteins in neurodegenerative diseases. *Mol Neurodegener*, **17**, 1–17.

70. Hirsch-Reinshagen, V., Pottier, C., Nicholson, A.M., Baker, M., Hsiung, G.Y.R., Krieger, C., Sengdy, P., Boylan, K.B., Dickson, D.W., Mesulam, M., *et al.* (2017) Clinical and neuropathological features of ALS/FTD with TIA1 mutations. *Acta Neuropathol Commun*, **5**, 96.

71. Montalbano, M., McAllen, S., Sengupta, U., Puangmalai, N., Bhatt, N., Ellsworth, A. and Kayed, R. (2019) Tau oligomers mediate aggregation of RNA-binding proteins Musashi1 and Musashi2 inducing Lamin alteration. *Aging Cell*, **18**, e13035.

72. Basha, M.R., Wei, W., Bakheet, S.A., Benitez, N., Siddiqi, H.K., Ge, Y.W., Lahiri, D.K. and Zawia, N.H. (2005) The fetal basis of amyloidogenesis: Exposure to lead and latent overexpression of amyloid precursor protein and β-amyloid in the aging brain. *Journal of Neuroscience*, **25**, 823–829.

73. Lin, Y., Protter, D.S.W., Rosen, M.K. and Parker, R. (2015) Formation and Maturation of Phase-Separated Liquid Droplets by RNA-Binding Proteins. *Mol Cell*, **60**, 208–219.

74. Molliex, A., Temirov, J., Lee, J., Coughlin, M., Kanagaraj, A.P., Kim, H.J., Mittag, T. and Taylor, J.P. (2015) Phase Separation by Low Complexity Domains Promotes Stress Granule Assembly and Drives Pathological Fibrillization. *Cell*, **163**, 123–133.

75. Murakami, T., Qamar, S., Lin, J.Q., Schierle, G.S.K., Rees, E., Miyashita, A., Costa, A.R., Dodd, R.B., Chan, F.T.S., Michel, C.H., *et al.* (2015) ALS/FTD Mutation-Induced Phase Transition of FUS Liquid Droplets and Reversible Hydrogels into Irreversible Hydrogels Impairs RNP Granule Function. *Neuron*, **88**, 678–690.

76. Patel, A., Lee, H.O., Jawerth, L., Maharana, S., Jahnel, M., Hein, M.Y., Stoynov, S., Mahamid, J., Saha, S., Franzmann, T.M., *et al.* (2015) A Liquid-to-Solid Phase Transition of the ALS Protein FUS Accelerated by Disease Mutation. *Cell*, **162**, 1066–1077.

77. Agrawal, S., Kuo, P.H., Chu, L.Y., Golzarroshan, B., Jain, M. and Yuan, H.S. (2019) RNA recognition motifs of disease-linked RNA-binding proteins contribute to amyloid formation. *Sci Rep*, **9**.

78. Kametani, F., Obi, T., Shishido, T., Akatsu, H., Murayama, S., Saito, Y., Yoshida, M. and Hasegawa, M. (2016) Mass spectrometric analysis of accumulated TDP-43 in amyotrophic lateral sclerosis brains. *Sci Rep*, **6**.

79. Li, Y. and Sun, S. (2025) RNA dysregulation in neurodegenerative diseases. *EMBO J*, **44**, 613–638.

80. Polymenidou, M., Lagier-Tourenne, C., Hutt, K.R., Huelga, S.C., Moran, J., Liang, T.Y., Ling, S.C., Sun, E., Wancewicz, E., Mazur, C., *et al.* (2011) Long pre-mRNA depletion and RNA missplicing contribute to neuronal vulnerability from loss of TDP-43. *Nat Neurosci*, **14**, 459–468.

81. Chen, P.C., Han, X., Shaw, T.I., Fu, Y., Sun, H., Niu, M., Wang, Z., Jiao, Y., Teubner, B.J.W., Eddins, D., *et al.* (2022) Alzheimer's disease-associated U1 snRNP splicing dysfunction causes neuronal hyperexcitability and cognitive impairment. *Nat Aging*, **2**, 923–940.

82. Stillman, B. and Stewart, D. (2007) Regulatory RNAs. *Cold Spring Harbor Laboratory Press*, **978**, 313–320.

83. Bai, B., Hales, C.M., Chen, P.C., Gozal, Y., Dammer, E.B., Fritz, J.J., Wang, X., Xia, Q., Duong, D.M., Street, C., *et al.* (2013) U1 small nuclear ribonucleoprotein complex and RNA splicing alterations in Alzheimer's disease. *Proc Natl Acad Sci U S A*, **110**, 16562–16567.

84. Lotti, F., Imlach, W.L., Saieva, L., Beck, E.S., Hao, L.T., Li, D.K., Jiao, W., Mentis, G.Z., Beattie, C.E., McCabe, B.D., *et al.* (2012) An SMN-dependent U12 splicing event essential for motor circuit function. *Cell*, **151**, 440–454.

85. Wu, R., Ye, Y., Dong, D., Zhang, Z., Wang, S., Li, Y., Wright, N., Redding-Ochoa, J., Chang, K., Xu, S., *et al.* (2024) Disruption of nuclear speckle integrity dysregulates RNA splicing in C9ORF72-FTD/ALS. *Neuron*, **112**, 3434–3451.

86. Sun, M., Bell, W., LaClair, K.D., Ling, J.P., Han, H., Kageyama, Y., Pletnikova, O., Troncoso, J.C., Wong, P.C. and Chen, L.L. (2017) Cryptic exon incorporation occurs in Alzheimer's brain lacking TDP-43 inclusion but exhibiting nuclear clearance of TDP-43. *Acta Neuropathol*, **133**, 923–931.

87. Vatsavayai, S.C., Jin Yoon, S., Gardner, R.C., Gendron, T.F., Norberto Vargas, J.S., Trujillo, A., Pribadi, M., Phillips, J.J., Gaus, S.E., Hixson, J.D., *et al.* (2016) Timing and significance of pathological features in C9orf72 expansion-associated frontotemporal dementia. *Brain*, **139**, 3202–3216.

88. Li, D., McIntosh, C.S., Mastaglia, F.L., Wilton, S.D. and Aung-Htut, M.T. (2021) Neurodegenerative diseases: a hotbed for splicing defects and the potential therapies. *Transl Neurodegener*, **10**.

89. Kraemer, B.C., Schuck, T., Wheeler, J.M., Robinson, L.C., Trojanowski, J.Q., Lee, V.M.Y. and Schellenberg, G.D. (2010) Loss of Murine TDP-43 disrupts motor function and plays an essential role in embryogenesis. *Acta Neuropathol*, **119**, 409–419.

90. Ash, P.E.A., Zhang, Y.J., Roberts, C.M., Saldi, T., Hutter, H., Buratti, E., Petrucelli, L. and Link, C.D. (2010) Neurotoxic effects of TDP-43 overexpression in C. elegans. *Hum Mol Genet*, **19**, 3206–3218.

91. Wils, H., Kleinberger, G., Janssens, J., Pereson, S., Joris, G., Cuijt, I., Smits, V., Ceuterick-De Groote, C., Van Broeckhoven, C. and Kumar-Singh, S. (2010) TDP-43 transgenic mice develop spastic paralysis and neuronal inclusions characteristic of ALS and frontotemporal lobar degeneration. *Proc Natl Acad Sci U S A*, **107**, 3858–3863.

92. Ayala, Y.M., Zago, P., D'Ambrogio, A., Xu, Y.F., Petrucelli, L., Buratti, E. and Baralle, F.E. (2008) Structural determinants of the cellular localization and shuttling of TDP-43. *J Cell Sci*, **121**, 3778–3785.

93. Huang, Y.C., Lin, K.F., He, R.Y., Tu, P.H., Koubek, J., Hsu, Y.C. and Huang, J.J.T. (2013) Inhibition of TDP-43 Aggregation by Nucleic Acid Binding. *PLoS One*, **8**, e64002.

94. Buratti, E. and Baralle, F.E. (2011) TDP-43: New aspects of autoregulation mechanisms in RNA binding proteins and their connection with human disease. *FEBS Journal*, **278**, 3530–3538.

95. Prasad, A., Bharathi, V., Sivalingam, V., Girdhar, A. and Patel, B.K. (2019) Molecular mechanisms of TDP-43 misfolding and pathology in amyotrophic lateral sclerosis. *Front Mol Neurosci*, **12**.

96. Zacco, E., Graña-Montes, R., Martin, S.R., de Groot, N.S., Alfano, C., Tartaglia, G.G. and Pastore, A. (2019) RNA as a key factor in driving or preventing self-assembly of the TAR DNA-binding protein 43. *J Mol Biol*, **431**, 1671–1688.

97. Watanabe, S., Oiwa, K., Murata, Y., Komine, O., Sobue, A., Endo, F., Takahashi, E. and Yamanaka, K. (2020) ALS-linked TDP-43M337V knock-in mice exhibit splicing deregulation without neurodegeneration. *Mol Brain*, **13**.

98. Ling, J., Pletnikova, O., Troncoso, J. and Wong, P. (2015) TDP-43 repression of nonconserved cryptic exon is compromised in ALS-FTD. *Science (1979)*, **349**, 650–655.

99. Baughn, M.W., Melamed, Z., López-Erauskin, J., Beccari, M.S., Ling, K., Zuberi, A., Presa, M., Gonzalo-Gil, E., Maimon, R., Vazquez-Sanchez, S., *et al.* (2023) Mechanism of STMN2 cryptic splice-polyadenylation and its correction for TDP-43 proteinopathies. *Science (1979)*, **379**, 1140–1149.

100. Liu, Y., Yan, D., Yang, L., Chen, X., Hu, C. and Chen, M. (2024) Stathmin 2 is a potential treatment target for TDP-43 proteinopathy in amyotrophic lateral sclerosis. *Transl Neurodegener*, **13**.

101. Keuss, M.J., Harley, P., Ryadnov, E., Jackson, R.E., Zanovello, M., Wilkins, O.G., Barattucci, S., Mehta, P.R., Oliveira, M.G., Parkes, J.E., *et al.* (2024) Loss of TDP-43 induces synaptic dysfunction that is rescued by UNC13A splice-switching ASOs. *bioRxiv*.

102. Agra Almeida Quadros, A.R., Li, Z., Wang, X., Ndayambaje, I.S., Aryal, S., Ramesh, N., Nolan, M., Jayakumar, R., Han, Y., Stillman, H., *et al.* (2024) Cryptic splicing of stathmin-2 and UNC13A mRNAs is a pathological hallmark of TDP-43-associated Alzheimer's disease. *Acta Neuropathol*, **147**.

103. Hsieh, Y.C., Guo, C., Yalamanchili, H.K., Abreha, M., Al-Ouran, R., Li, Y., Dammer, E.B., Lah, J.J., Levey, A.I., Bennett, D.A., *et al.* (2019) Tau-Mediated Disruption of the Spliceosome Triggers Cryptic RNA Splicing and Neurodegeneration in Alzheimer's Disease. *Cell Rep*, **29**, 301-316.e10.

104. Fang, W.Q., Chen, W.W., Jiang, L., Liu, K., Yung, W.H., Fu, A.K.Y. and Ip, N.Y. (2014) Overproduction of Upper-Layer Neurons in the Neocortex Leads to Autism-like Features in Mice. *Cell Rep*, **9**, 1635–1643.

105. Cheng, N., Alshammari, F., Hughes, E., Khanbabaei, M. and Rho, J.M. (2017) Dendritic overgrowth and elevated ERK signaling during neonatal development in a mouse model of autism. *PLoS One*, **12**, e0179409.

106. Skelton, P.D., Stan, R.V. and Luikart, B.W. (2019) The Role of PTEN in Neurodevelopment. *Complex Psychiatry*, **5**, 60–71.

107. Capizzi, M., Carpentier, R., Denarier, E., Adrait, A., Kassem, R., Mapelli, M., Couté, Y. and Humbert, S. (2022) Developmental defects in Huntington's disease show that axonal growth and microtubule reorganization require NUMA1. *Neuron*, **110**, 36-50.e5.

108. Schindlbeck, K.A., Vo, A., Nguyen, N., Tang, C.C., Niethammer, M., Dhawan, V., Brandt, V., Saunders-Pullman, R., Bressman, S.B. and Eidelberg, D. (2020) LRRK2 and GBA Variants Exert Distinct Influences on Parkinson's Disease-Specific Metabolic Networks. *Cerebral Cortex*, **30**, 2867–2878.

109. Schaefer, A.M., Sanes, J.R. and Lichtman, J.W. (2005) A compensatory subpopulation of motor neurons in a mouse model of amyotrophic lateral sclerosis. *Journal of Comparative Neurology*, **490**, 209–219.

110. Fischer, L.R., Culver, D.G., Tennant, P., Davis, A.A., Wang, M., Castellano-Sanchez, A., Khan, J., Polak, M.A. and Glass, J.D. (2004) Amyotrophic lateral sclerosis is a distal axonopathy: Evidence in mice and man. *Exp Neurol*, **185**, 232–240.

111. Lule, D., Ludolph, A.C. and Ludolph, A.G. (2008) Neurodevelopmental and neurodegenerative diseases - Is there a pathophysiological link? Attention-deficit/hyperactivity disorder and amyotrophic lateral sclerosis as examples. *Med Hypotheses*, **70**, 1133–1138.

112. Devenney, E.M., Ahmed, R.M., Halliday, G., Piguet, O., Kiernan, M.C. and Hodges, J.R. (2018) Psychiatric disorders in *C9orf72* kindreds. *Neurology*, **91**, 1498–1507.

113. Watson, A., Pribadi, M., Chowdari, K., Clifton, S., Joel Wood, Miller, B.L., Coppola, G. and Nimgaonkar, V. (2016) C9orf72 repeat expansions that cause frontotemporal dementia are detectable among patients with psychosis. *Psychiatry Res*, **235**, 200–202.

114. Usui, N., Kobayashi, H. and Shimada, S. (2023) Neuroinflammation and Oxidative Stress in the Pathogenesis of Autism Spectrum Disorder. *Int J Mol Sci*, **24**, 5487.

115. Blanco, S., Dietmann, S., Flores, J. V, Hussain, S., Kutter, C., Humphreys, P., Lukk, M., Lombard, P., Treps, L., Popis, M., *et al.* (2014) Aberrant methylation of t RNA s links cellular stress to neuro-developmental disorders . *EMBO J*, **33**, 2020–2039.

116. Dong, D., Zielke, H.R., Yeh, D. and Yang, P. (2018) Cellular stress and apoptosis contribute to the pathogenesis of autism spectrum disorder. *Autism Research*, **11**, 1076–1090.

Table 1: Primers used for RT-PCR experiments.

Gene	Primer Sequences
TDP-43	F: 5'- ATGTCTGAATATATTCGGGTAACCGAAG-3' R: 5'-CTACATTCCCCAGCCAGAAGACTTAG-3'
Poldip3 (4)	F: 5'-TGCTCTGAAGCTCACCAAAA-3' R: 5'-AAGTGGTCGTTGAGGGCAAT-3'
GAPDH	F: 5'-ACCATCTTCCAGGAGCGAGAT-3' R: 5'-AAGTGGTCGTTGAGGGCAAT-3'
ACTIN	F: 5'-AGAAAATCTGGCACCACACC-3' R: 5'-GGGGTGTTGAAGGTCTCAAA-3'
NMNAT2	F: 5'-GACCACCAAGACCCACGTTA-3' R: 5'-CAGCAGGATCCGTAGCTCAAT-3'
NRXN2	F: 5'-CAGCCGCAAGGTCAATGATG-3' R: 5'-CTCCAGGTCCAGAATCTCGC-3'
PTPRN2	F: 5'- TGGAGTGTTTGGAAGGTGCC-3' R: 5'-GAAGCGGTCATCACCCTCAG-3'
GRIN1	F: 5'-CGTGAGTCCAAGGCAGAGAA-3' R: 5'-TAGATGCCCACTTGCACCAG-3'
C1QL1	F: 5'-GGCGGCAACAGCAACAAATA-3' R: 5'-AATATATAGCGCGGGCTGGG-3'
SLIT1	F: 5'-CAGCGGCTATAAGGGTCGAG-3' R: 5'-GCCAGTTTTGCAGGTCAGTG-3'
SEZ6L	F: 5'-GTGGGGACCACCATCCAATA-3' R: 5'-TGCCGCTTCTGCTACTTCTAA-3'
GABRB3	F: 5'-ACGGTGGACAAGCTGTTGAA-3' R: 5'-AGCACAGTTGTGATCCCGAG-3'
TIMP1	F: 5'-AGAGAGACACCAGAGAACCC-3' R: 5'-GCATCCCCTAAGGCTTGGAA-3'
COL3A1	F: 5'-CGCCCTCCTAATGGTCAAGG-3' R: 5'-TCCATCGAAGCCTCTGTGTC-3'
NKX2-5	F: 5'-GCCGAAAAGAAAGAGCTGTGC-3' R: 5'-TCCCTACCAGGCTCGGATAC-3'
S100A10	F: 5'-CACGTACTAAGGAAGGCGCA-3' R: 5'-GCCAGAGGGTCTTTTTGATTTTCC-3'
CCDC80	F: 5'-CACGCAGAGTCCCAAGAAGT-3' R: 5'-CAAAATTGCACGCCTGACCA-3'
S100A11	F: 5'-GCTCAGCTCCAACATGGCAAAA-3' R: 5'-CTTCTGGGAAGGGACAGCCT-3'
STMN2	F: 5'-CAGCGTCTGCACATCCCTA-3' R: 5'-CGCAGCATGCCTCTCCTTT-3'
UNC13A	F: 5'-CAAGCCACTCAGACGGAACC-3' R: 5'-GGTCGCAAACTTGCGTTTCT-3'
β-III Tubulin	F: 5'-TGGATCCCCAACAACGTGAA-3' R: 5'-TTCGTACATCTCGCCCTCTTC-3'
MAP2	F: 5'-AGGCTGTAGCAGTCCTGAAAGG-3' R: 5'-CTTCCTCCACTGTGACAGTCTG-3'

Figure 1: Generating CRISPR-edited K181E or K263E-TDP-43 cells. A. The design to introduce K181E and K263E substitution via CRIPSR-editing. Nucleotides encoding K181 and K263 are localised in exon 4 and 6 respectively on TARDBP gene. The position of gRNA, PAM sequence and expected Cas9 cut sites are shown. The gRNAs are highlighted and shown in blue, within which the nucleotide changes for K181E and K263E are highlighted in red. The PAM sequence (AGG or CGG) is immediately downstream of the gRNA alignment site, the expected cut site is indicated with the red arrow head. The sequence used of ssODN is also displayed, with the nucleotide changes for K181E and K263E highlighted in red, and silence mutations in gold. **B.** Staining of TDP-43 of unmodified WT or CRISPR/Cas 9-edited mutant SH-SY5Y cells. Images taken on Zeiss LSM 880 confocal using 63X oil lens. Scale bar = 25µM. **C.** Quantification of cells with cleaved caspase-3 staining (%). 100 cells were counted per condition per experiment, N=3-5. Means and SDs are shown**.** The data was analysed by One-way ANOVA followed by Dunnet's post-test. ns = not significant, * $p<0.05$.

Figure 2: Polarised DEGs in K181E-TDP-43 homozygous and heterozygous cells. A-B. Volcano plots showing genes with significantly altered expression in K181E-TDP-43 homozygous cells (A) or heterozygous cells (B) relative to un-edited control SH-SY5Y cells. DEGs highlighted in pink were identified with a cut-off of 0.1 for adjusted *p* values (-Log10(q<0.1)) and a total cut-off of 1 for the log2 fold change ratio. **C.** Heatmap comparing the DEGs level across conditions. All DEGs identified in K181E-TDP-43 homozygous vs WT(B) and K181E-TDP-43 heterozygous vs WT (C) are plotted in the heatmap. The colour scale shows transcripts that are upregulated (pink) or downregulated (blue) relative to mean expression of all samples (Z-score). **D.** Volcano plot showing genes with significantly altered expression in K181E homozygous compared to heterozygous cells. DEGs highlighted in pink were identified with a cut-off of 0.05 for adjusted *p* values (-Log10(q<0.05)) and a total cut-off of 1 for the log2 fold change ratio.

Figure 3: Neuronal and synaptic pathways identified as most significantly down-regulated in K181E-TDP-43 homozygous cells. A. Gene set enrichment analysis for DEGs down-regulated in K181E-TDP-43 homozygous cells (compared to K181E-TDP-43 heterozygous), using gene ontology biological processes and cellular components gene sets from MSigDB. πvalues (-log10(p-value) x log2(fold change)) were used as the rank of significance. The most significant gene ontology terms for biological processes and cellular components and associated genes are shown with the associated significance (-log10(Pvalue), shown in colour scale). Gene ratio = (Gene count from RNA-Seq data associated with pathway/ Total gene count within MSigDB pathway dataset). **B.** Log2 Fold Change plotted against Average TPMs for K181E homozygous compared with K181E heterozygous cells. Only DEGs were plotted ($q<0.05$, total log2 fold change of 1). Genes involved in neuronal pathways identified in gene set enrichment analysis are highlighted in pink. **C.** The frequency of biological processes highlighted in the GO term analysis of genes down-regulated in K181E-TDP-43 homozygous cells. **D.** Heatmap of the most significantly up- and down-regulated genes identified in the K181E-TDP-43 homozygous and heterozygous comparison. The three known TDP-43 targets, STMN2, UNC13A and NPTX2, are also in the comparison.

Figure 4: Isoform changes in neuronal genes as a result of K181E-TDP-43 mutations. A-B. Volcano plots generated from IsoformSwitchAnalyzeR showing significant isoform switches in K181E-TDP-43 homozygous cells (A) or heterozygous cells (B) relative to un-edited control SH-SY5Y cells. -Log10(q<0.05) plotted against difference in isoform fraction**.** Significant changes are recognised by an absolute difference in isoform fraction of 0.1, highlighted in yellow. **C.** Alternative splicing events caused by K181E-TDP-43 expression. The alternative splicing events are identified by IsoformSwitchAnalyzeR, analysing all transcript isoforms identified as significantly changed in (A) and (B). ATSS, Alternative Transcript Start Site; ATTS, Alternative Transcript Termination Site; IR, Intron Retention; ES, Exon Skipping; MES, Mutually Exclusive Exons; A5', Alternative 5' Splicing; A3', Alternative 3' Splicing. **D.** Volcano plot generated from IsoformSwitchAnalyzeR showing significant isoform switches between K181E-TDP-43 homozygous cells and heterozygous cells. Significant changes are recognised by an absolute difference in isoform fraction of 0.1, highlighted in yellow. **E.** Gene set enrichment analysis for significantly changed genes identified in (D), using gene ontology biological processes and cellular components gene sets from MSigDB. Gene set enrichment analysis used πvalues (-log10(p-value) x log2(fold change)) as the rank of significance. The most significant gene ontology terms for biological processes and cellular components and associated gene are shown with associated significance (shown in colour scale). Gene ratio= (Gene count from RNA-Seq dataset associated with pathway/ Total gene count within MSigDB pathway dataset). **F.** Shift of DCTN1 isoforms present in WT, K181E-TDP-43 homozygous and heterozygous cells. The fraction of *DCTN1-228, DCTN1-203* and other DCTN1 isoforms found in our RNA-seq dataset are plotted. Combined fractions of the remaining 26 *DCTN1* isoforms are illustrated in black. **G.** Heat map of gene expression reads (TPMs) for *DCTN1-228* and *DCTN1-203* from various brain regions obtained from GTex (https://gtexportal.org/home/), and our WT and K181E-TDP-43 datasets. Increased abundance indicated in pink, decreased abundance indicated in blue.

Figure 5: K181E-TDP-43 expression significantly affects neuronal differentiation and processing. A. Schematic for SH-SY5Y cell differentiation used in this study (made on BioRender.com). The differentiation is induced via the sequential addition of retinoic acid and BDNF. The RT-PCR and immunofluorescence staining of MAP2 and beta III-tubulin validated the differentiation. **B.** Immunofluorescence showing abundance of MAP2 positive cells in undifferentiated state, mid-differentiation (5 days after retinoic acid treatment) and fully differentiated (5 days after BDNF treatment). The proportion of MAP2 positive cells are quantified from three independent studies. Scale bar = 100μm. Means and SDs are shown. The data were analysed by Two-way ANOVA with Tukey's post-test. **C.** Expression of MAP2 is visualised and quantified by RT-PCR of endogenous MAP2 mRNA at different differentiation stages. RT-PCR of actin is used as loading control. The levels of MAP2 were quantified, normalised to the loading control, and presented in relation to WT. N=3. Means and SDs are shown. The data were analysed by Two-way ANOVA with Tukey's post-test. **D.** Sum neurite length from MAP2 staining from (B) was quantified for approximately 30 individual cells across three independent experiments for the individual clones. Means and SEMs are shown. The data were analysed by One-way ANOVA followed by Dunnet's post-test. **E.** Validation of the changes in genes-linked to neuronal development and progression identified in our K181E-TDP-43 RNA seq dataset. RT-PCR of selected genes identified in RNA-seq was carried out using RNA extracted from cells of undifferentiation or fully differentiation state. Known TDP-43 targets, STMN2 and UNC13A are also included in this study. Actin is used as a loading control. A representative RT-PCR result is shown here with the overall quantification and statistically comparison from 3 independent extractions shown in supplementary figure. ns = not significant, * $p<0.05$, ** $p<0.01$, *** $p<0.001$, **** $p<0.0001$.

A)

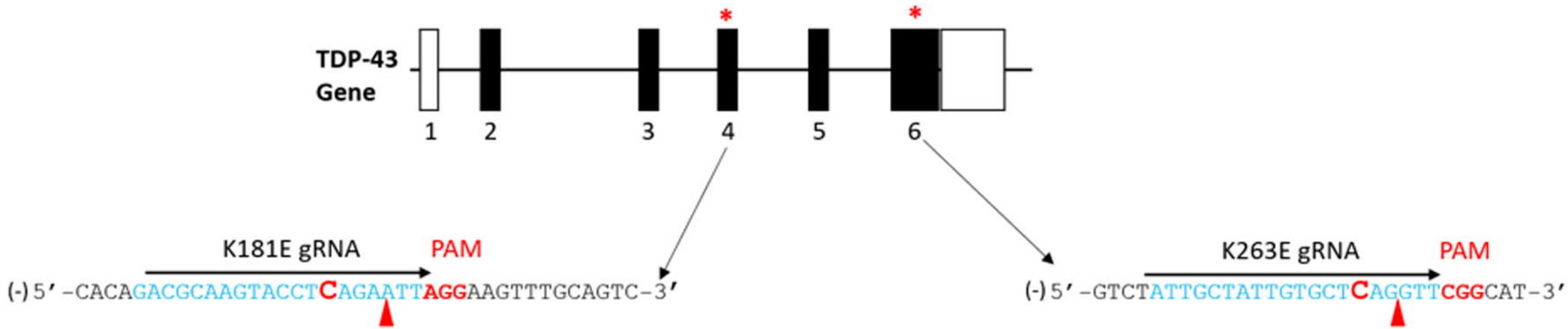

K181E ssODN (84bp):

(+) 5′TATGATAGATGGACGATGGTGTGACTGCAAACTTCCTAACTCTGAGG
TACTTGCGTCTGTGCTTTGGGAATTTTTGCCAACAAA3′

K263E ssODN (83bp):

(+) 5′ATCATTAAAGGAATCAGCGTTCATATATCCAATGCAGAACCTGAGCACAATAGCA
ATAGACAGTTAGAAAGAAGTGGAAGATT3′

B)

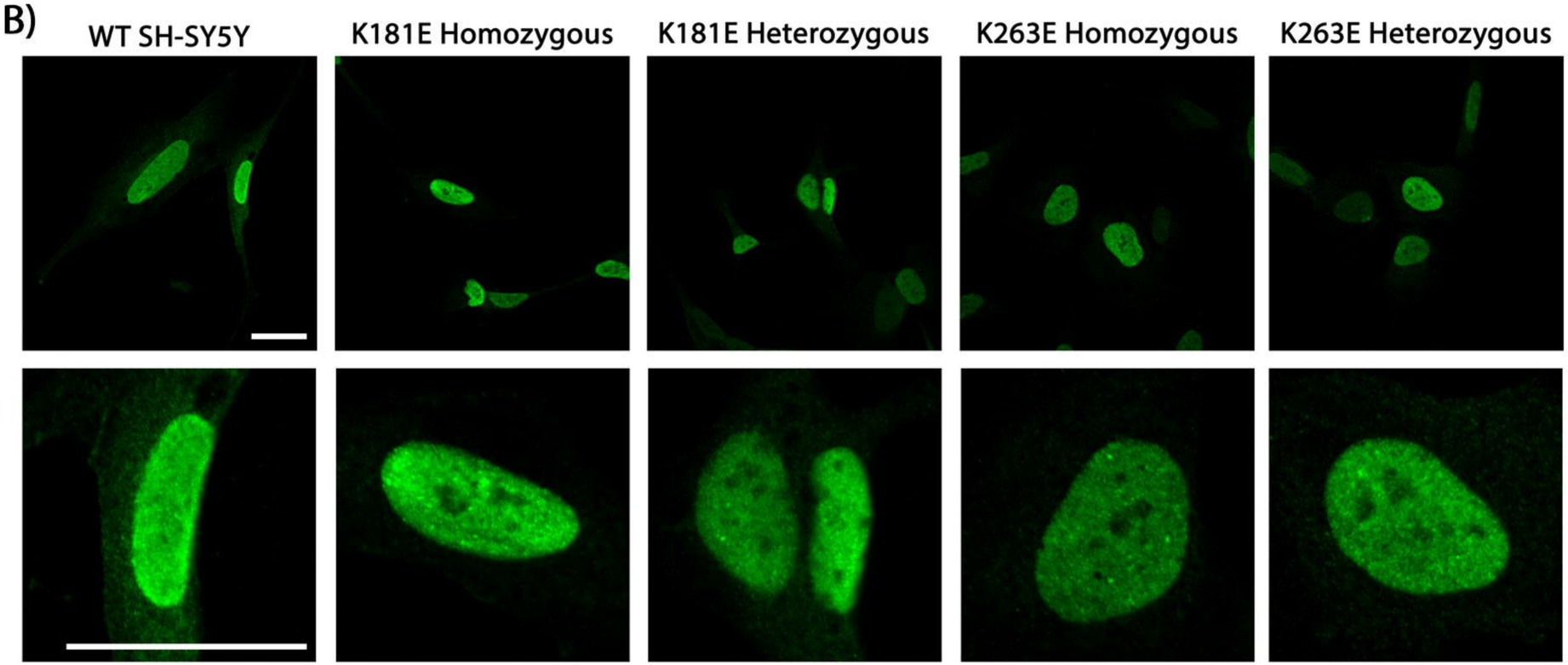

C)

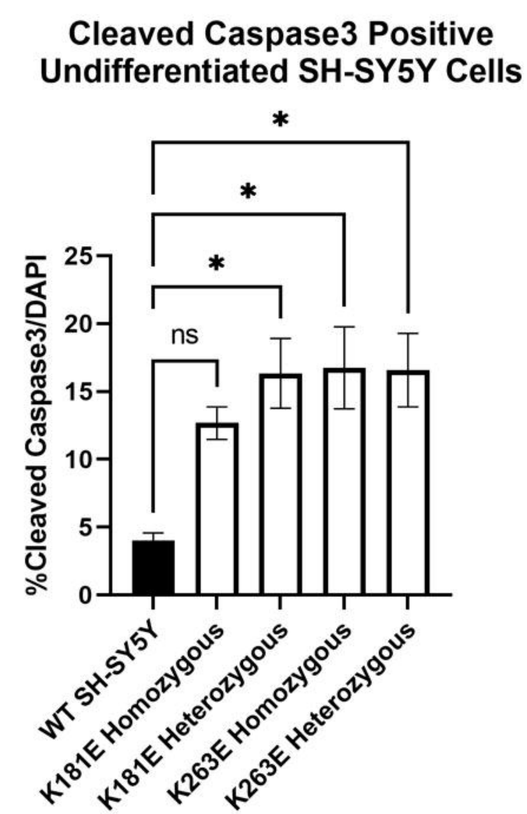

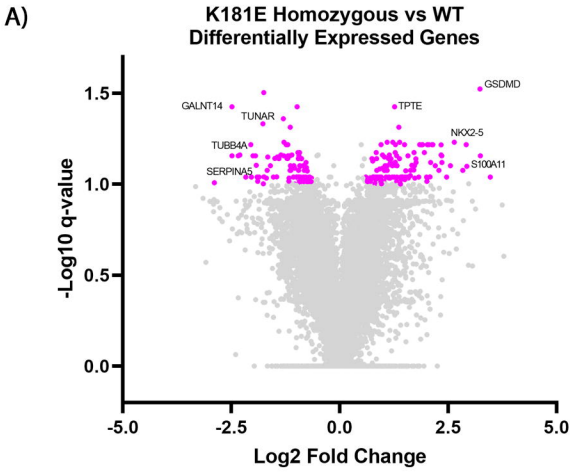
A)
K181E Homozygous vs WT
Differentially Expressed Genes
GSDMD
GALNT14
TUNAR
TPTE
NKX2-5
TUBB4A
S100A11
SERPINA5
-Log10 q-value
Log2 Fold Change

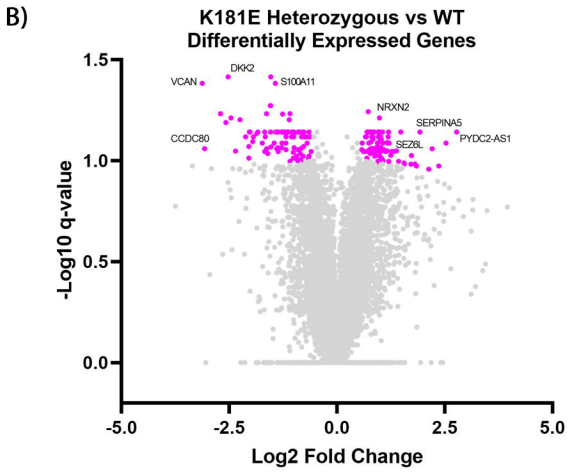
B)
K181E Heterozygous vs WT
Differentially Expressed Genes
DKK2
VCAN
S100A11
NRXN2
SERPINA5
CCDC80
PYDC2-AS1
SEZ6L
-Log10 q-value
Log2 Fold Change

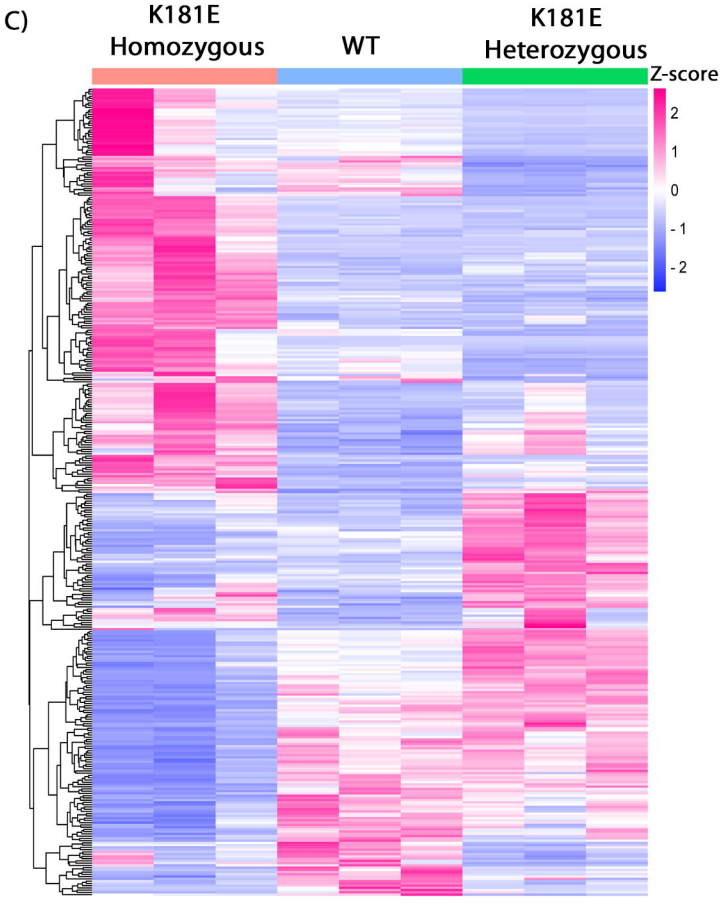
C)
K181E Homozygous
WT
K181E Heterozygous
Z-score
2
1
0
-1
-2

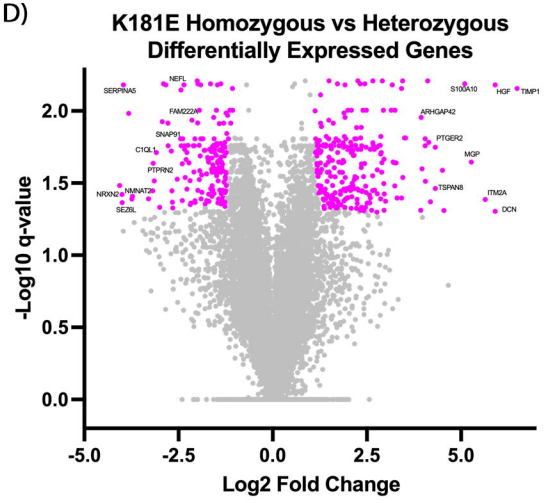
D)
K181E Homozygous vs Heterozygous
Differentially Expressed Genes
NEFL
SERPINA5
S100A10
HGF
TIMP1
FAM222A
ARHGAP42
SNAP91
PTGER2
C1QL1
MGP
PTPRN2
TSPAN8
NRXN2
NMNAT2
ITM2A
SEZ6L
DCN
-Log10 q-value
Log2 Fold Change

A)

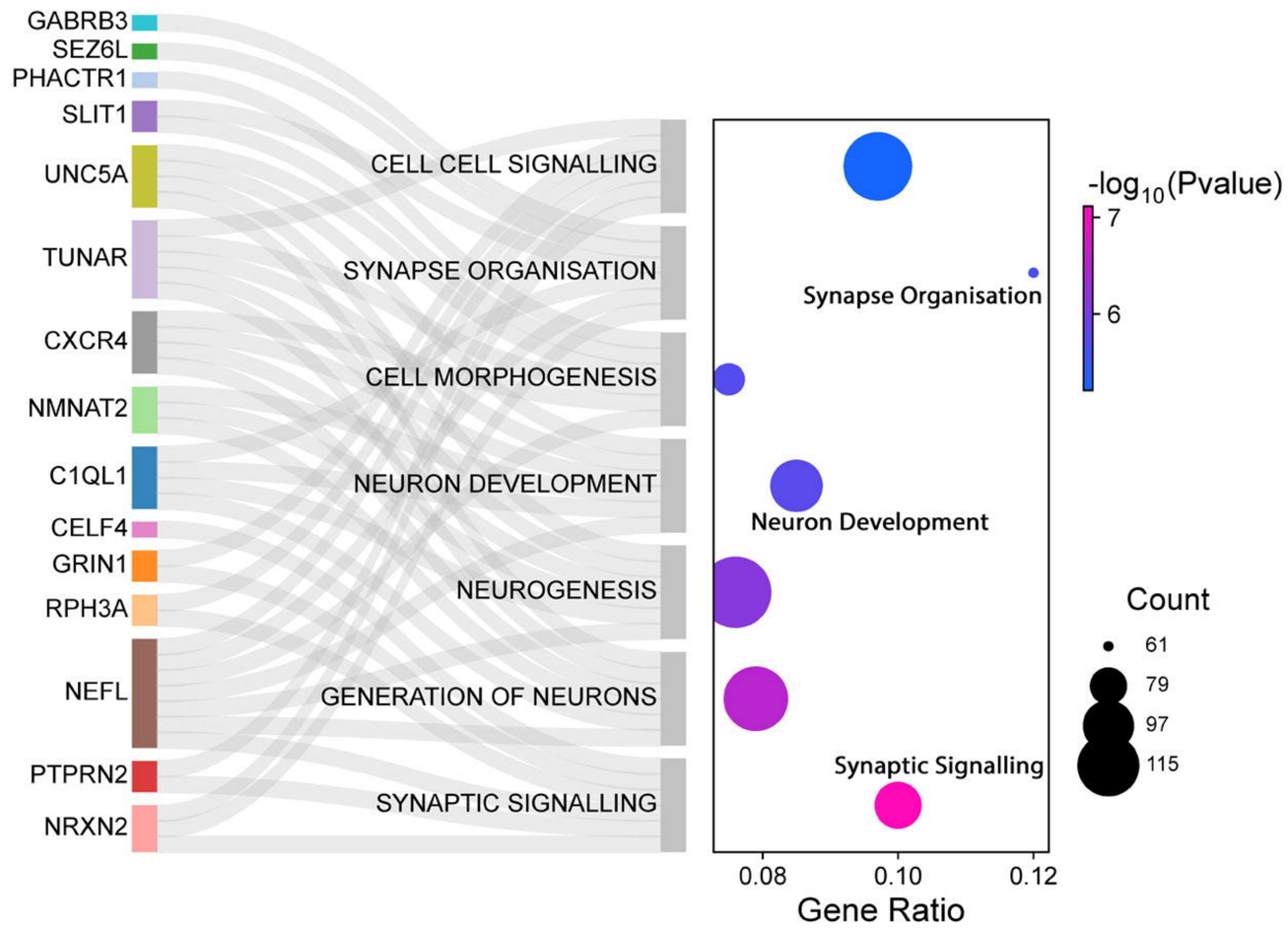

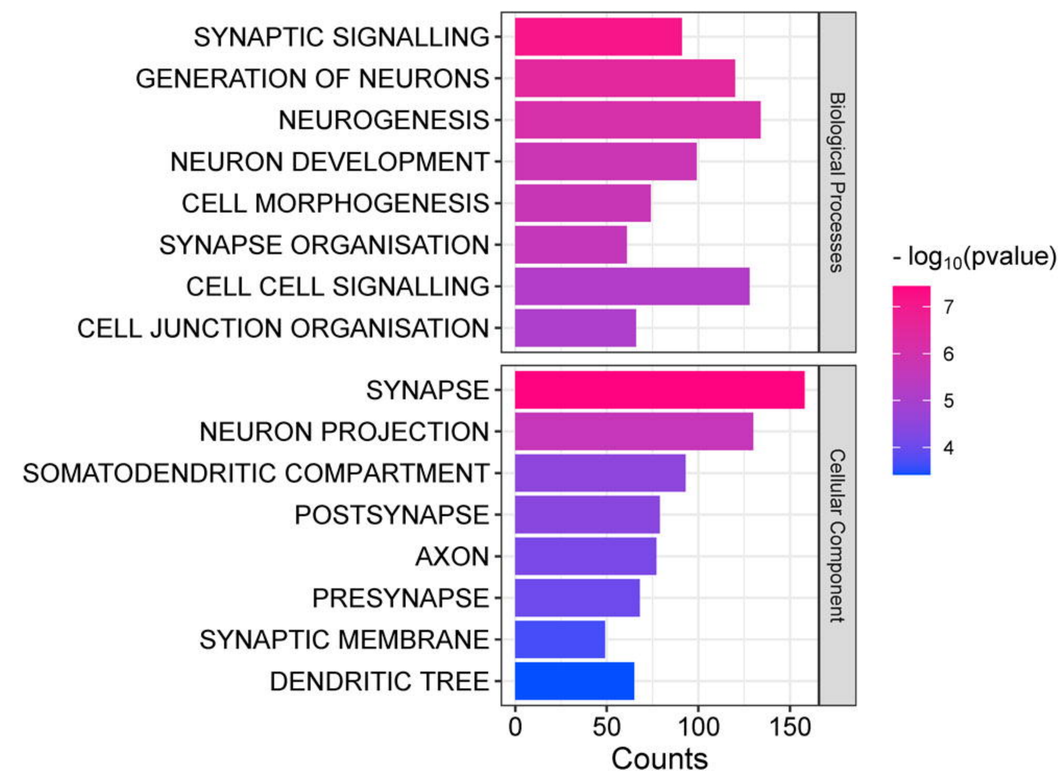

B)

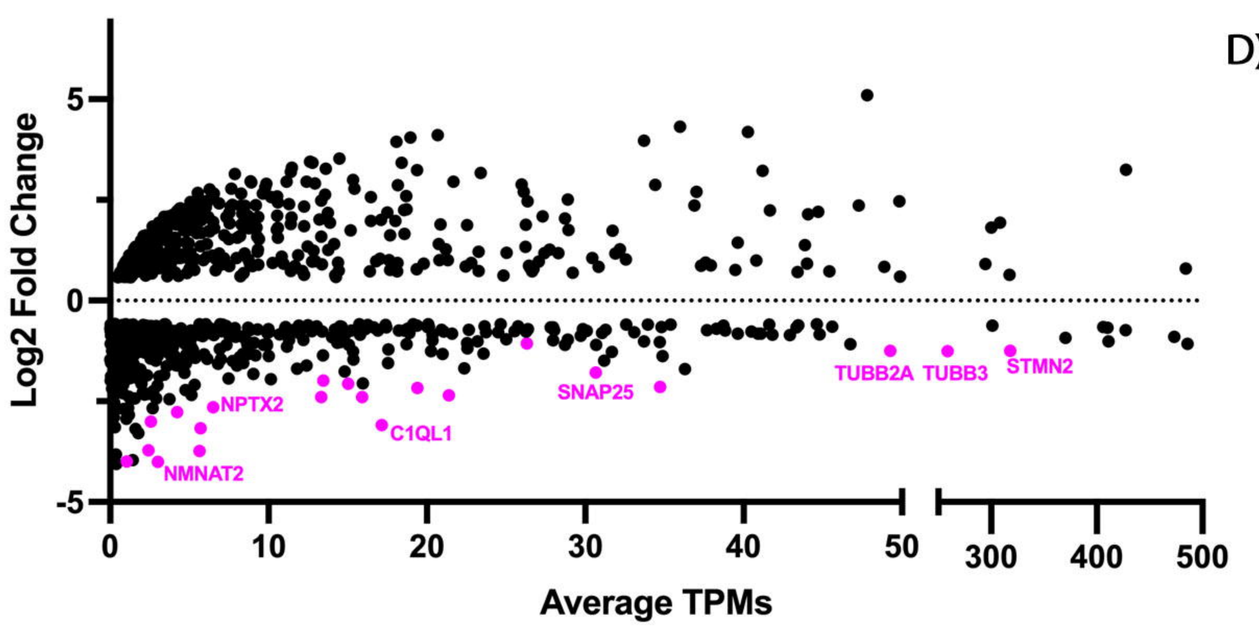

D)

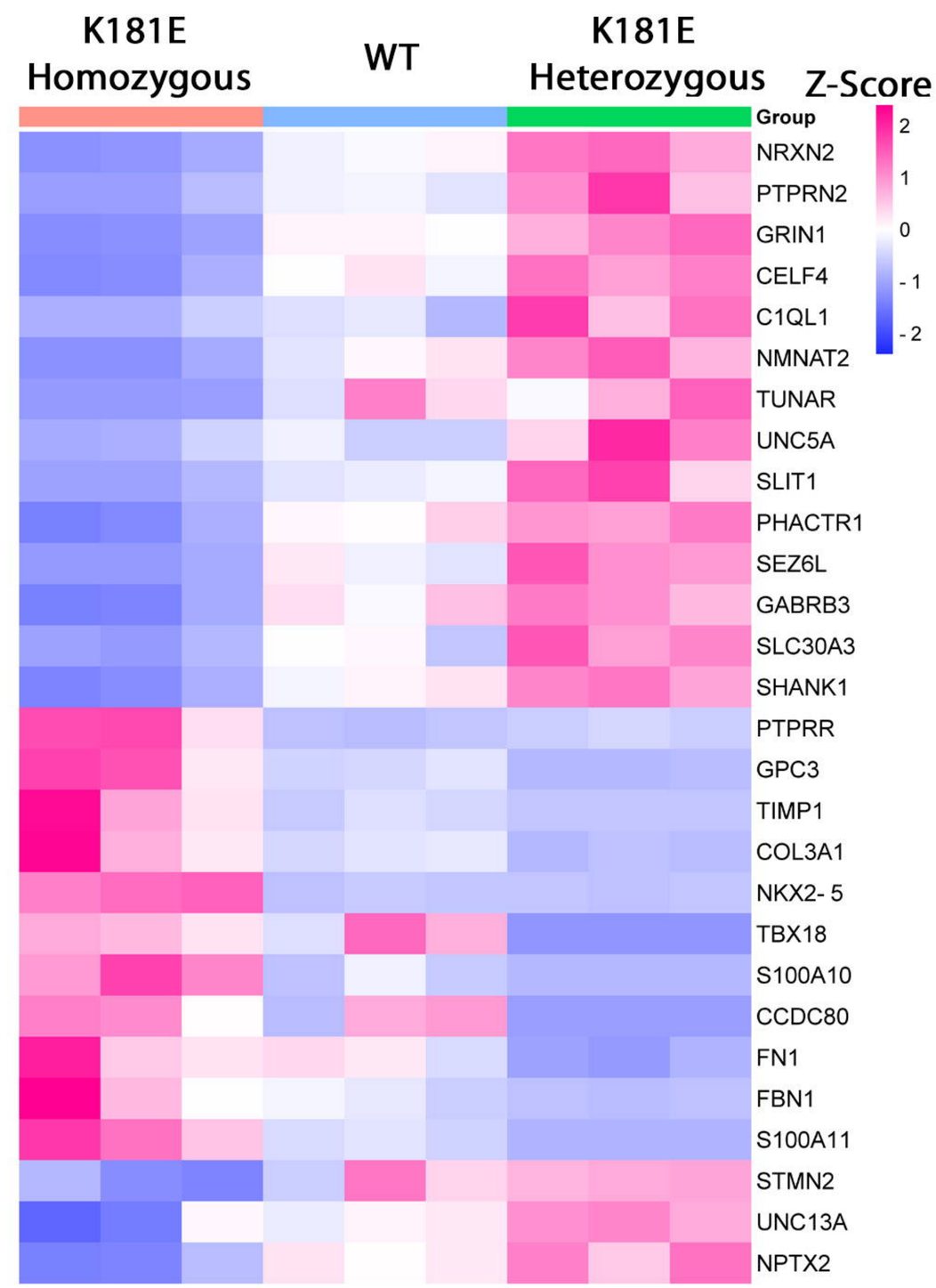

C) K181E-TDP-43 Homozygous Down-Regulated DEGs Biological Processes GO Terms

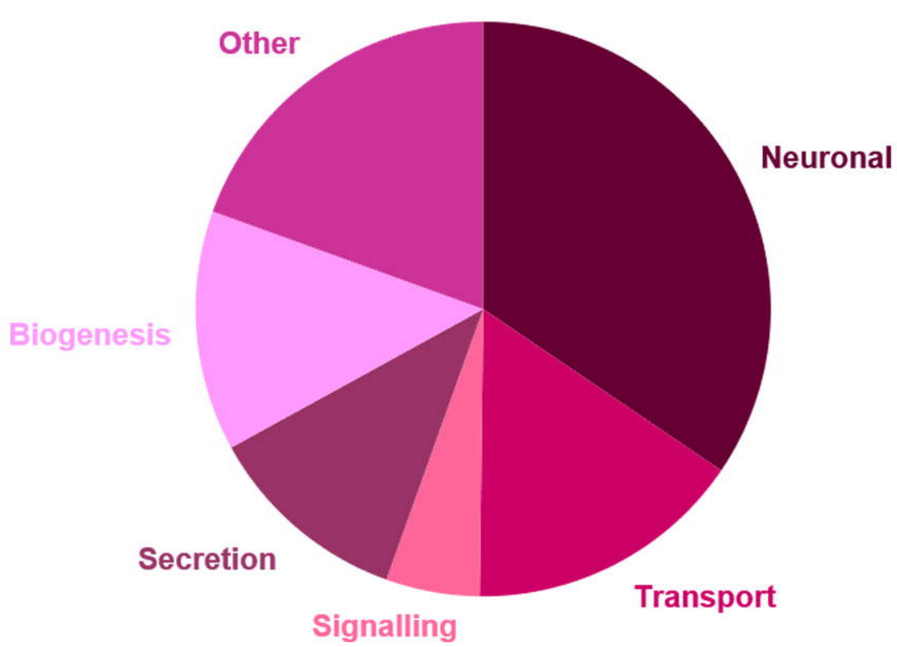

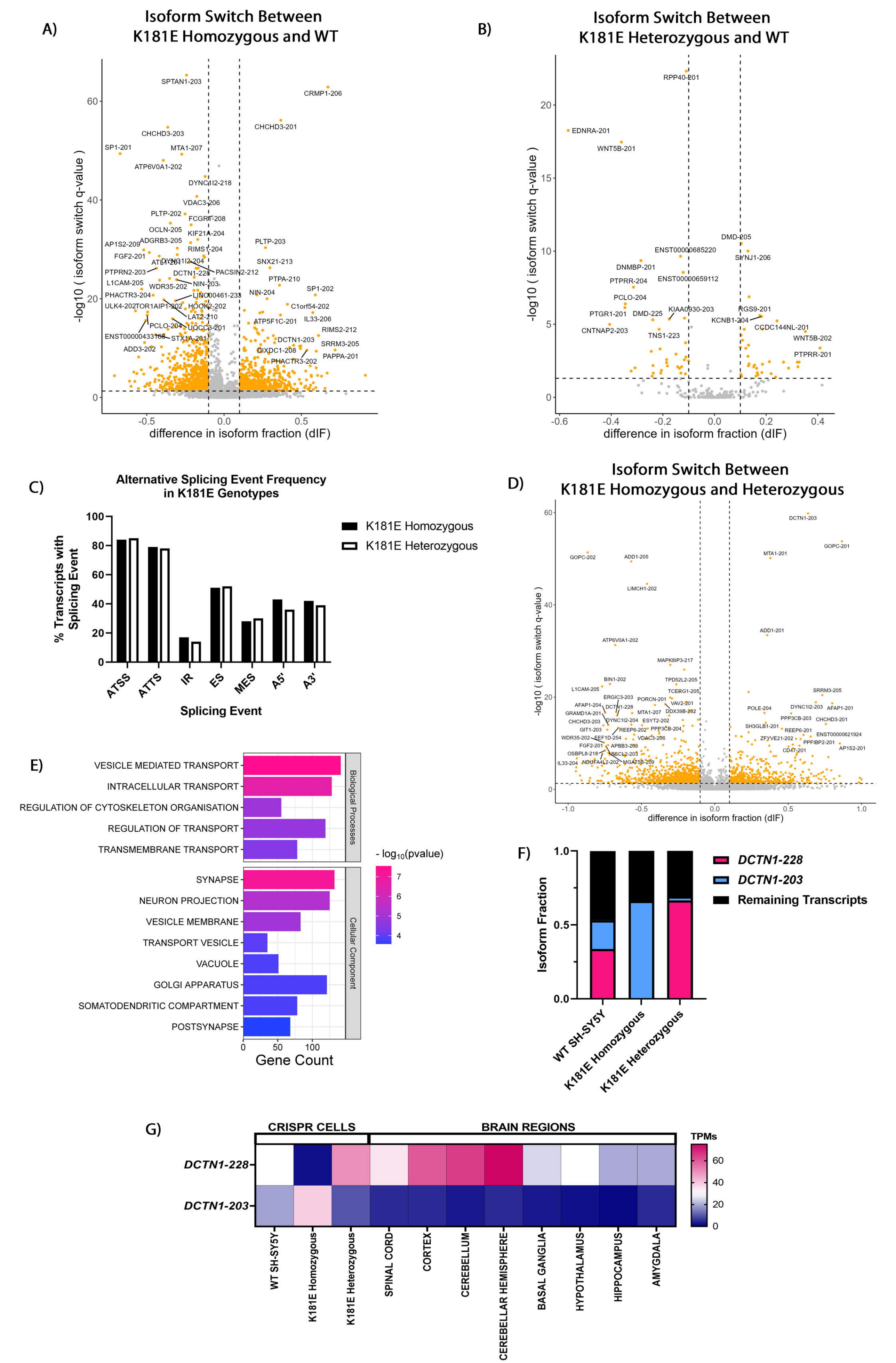
A)
Isoform Switch Between
K181E Homozygous and WT
-log10 (isoform switch q-value)
difference in isoform fraction (dIF)
B)
Isoform Switch Between
K181E Heterozygous and WT
-log10 (isoform switch q-value)
difference in isoform fraction (dIF)
C)
Alternative Splicing Event Frequency
in K181E Genotypes
% Transcripts with Splicing Event
K181E Homozygous
K181E Heterozygous
ATSS
ATTS
IR
ES
MES
A5'
A3'
Splicing Event
D)
Isoform Switch Between
K181E Homozygous and Heterozygous
-log10 (isoform switch q-value)
difference in isoform fraction (dIF)
E)
VESICLE MEDIATED TRANSPORT
INTRACELLULAR TRANSPORT
REGULATION OF CYTOSKELETON ORGANISATION
REGULATION OF TRANSPORT
TRANSMEMBRANE TRANSPORT
Biological Processes
SYNAPSE
NEURON PROJECTION
VESICLE MEMBRANE
TRANSPORT VESICLE
VACUOLE
GOLGI APPARATUS
SOMATODENDRITIC COMPARTMENT
POSTSYNAPSE
Cellular Component
- log10(pvalue)
Gene Count
F)
Isoform Fraction
DCTN1-228
DCTN1-203
Remaining Transcripts
WT SH-SY5Y
K181E Homozygous
K181E Heterozygous
G)
CRISPR CELLS
BRAIN REGIONS
TPMs
DCTN1-228
DCTN1-203
WT SH-SY5Y
K181E Homozygous
K181E Heterozygous
SPINAL CORD
CORTEX
CEREBELLUM
CEREBELLAR HEMISPHERE
BASAL GANGLIA
HYPOTHALAMUS
HIPPOCAMPUS
AMYGDALA

A)

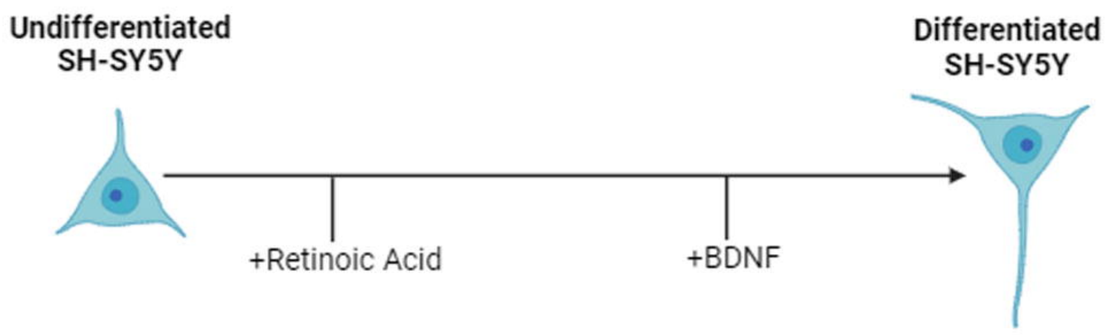
Undifferentiated
SH-SY5Y
Differentiated
SH-SY5Y
+Retinoic Acid
+BDNF

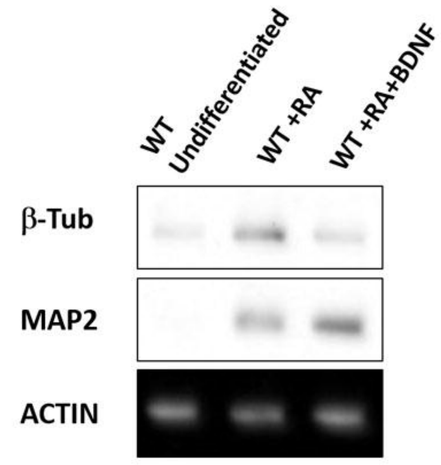
WT
Undifferentiated
WT +RA
WT +RA+BDNF
β-Tub
MAP2
ACTIN

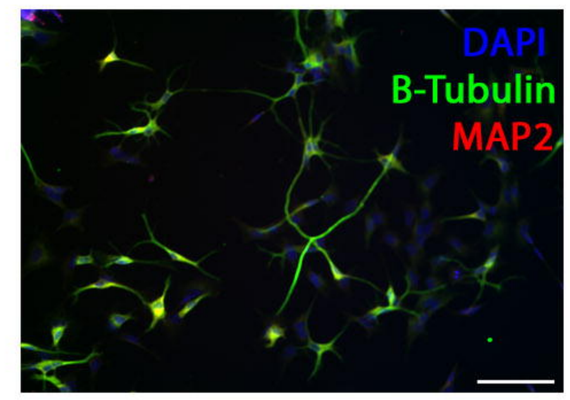
DAPI
B-Tubulin
MAP2

B)

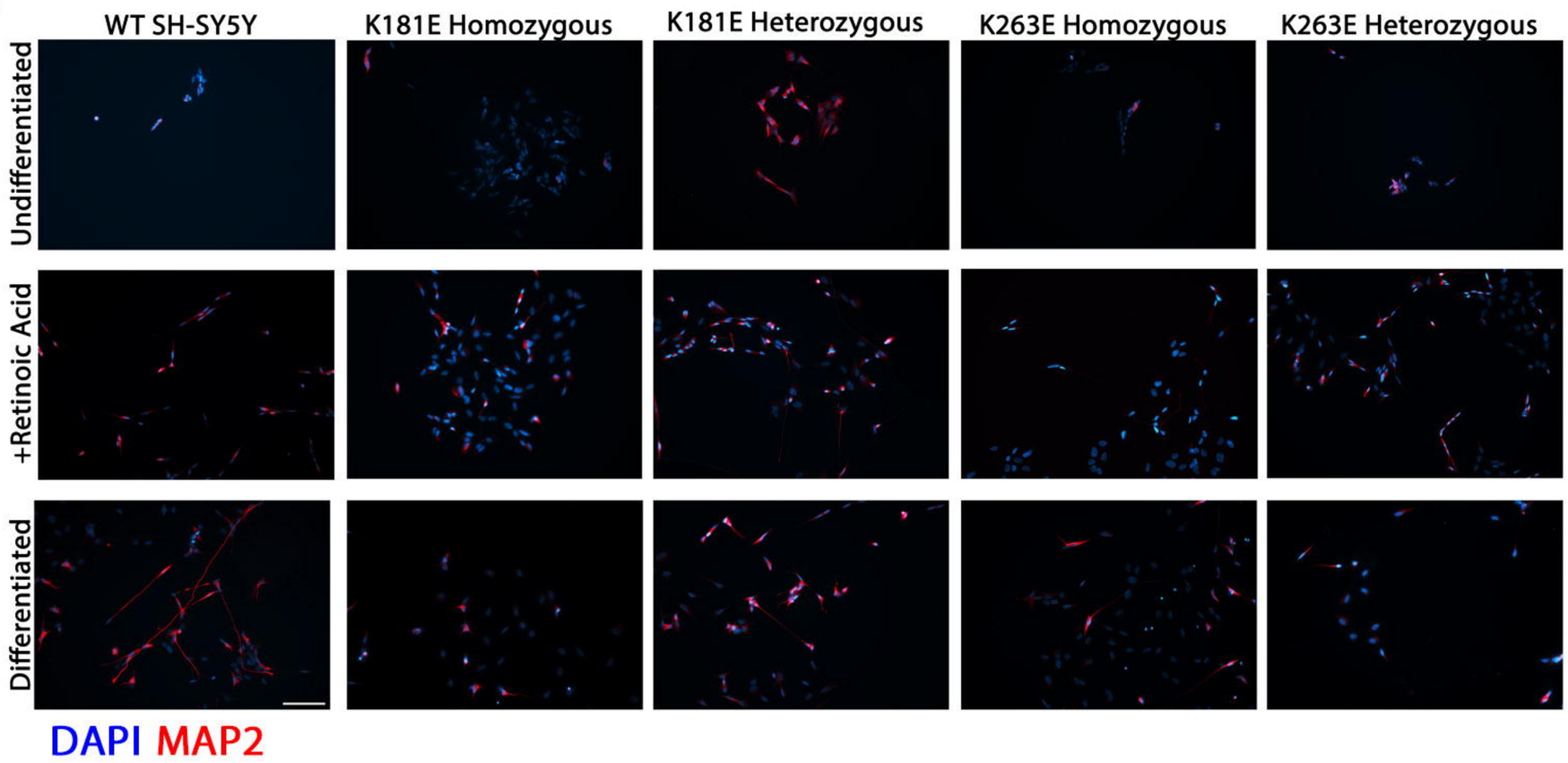
WT SH-SY5Y
K181E Homozygous
K181E Heterozygous
K263E Homozygous
K263E Heterozygous
Undifferentiated
+Retinoic Acid
Differentiated
DAPI MAP2

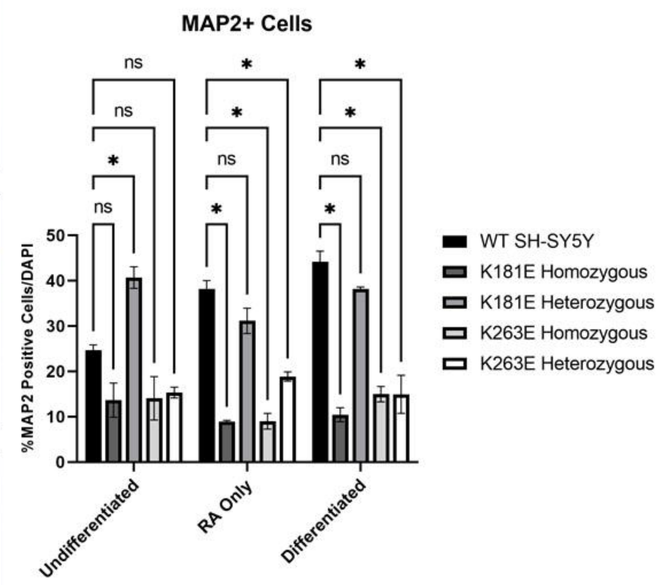
MAP2+ Cells
%MAP2 Positive Cells/DAPI
Undifferentiated
RA Only
Differentiated
WT SH-SY5Y
K181E Homozygous
K181E Heterozygous
K263E Homozygous
K263E Heterozygous

C)

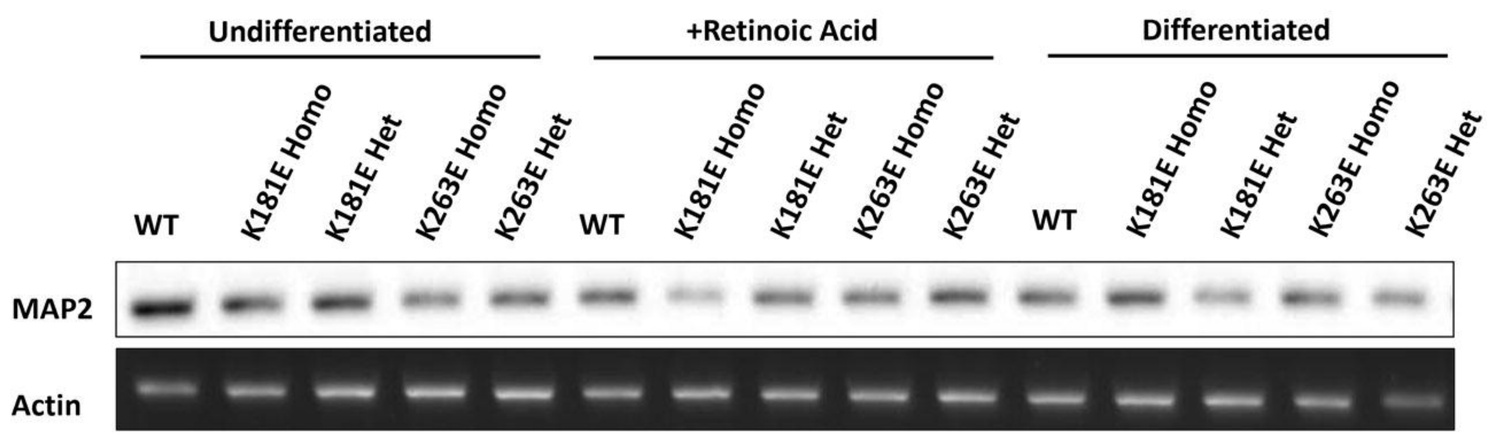
Undifferentiated
+Retinoic Acid
Differentiated
WT
K181E Homo
K181E Het
K263E Homo
K263E Het
MAP2
Actin

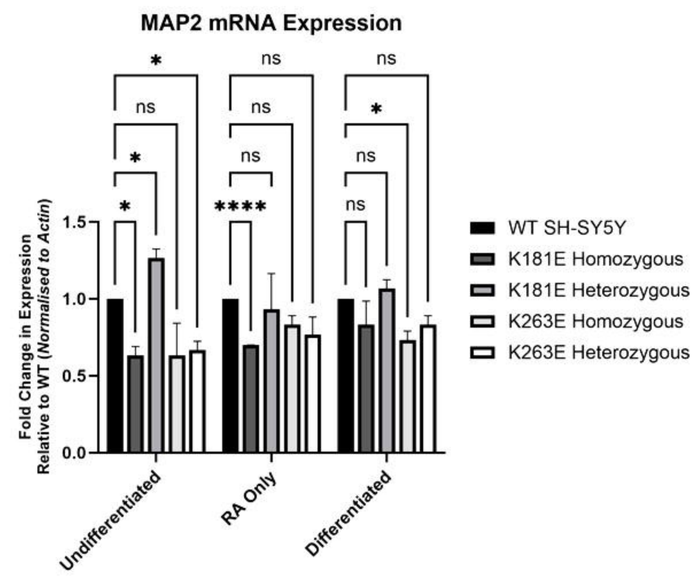
MAP2 mRNA Expression
Fold Change in Expression Relative to WT (Normalised to Actin)
Undifferentiated
RA Only
Differentiated
WT SH-SY5Y
K181E Homozygous
K181E Heterozygous
K263E Homozygous
K263E Heterozygous

D)

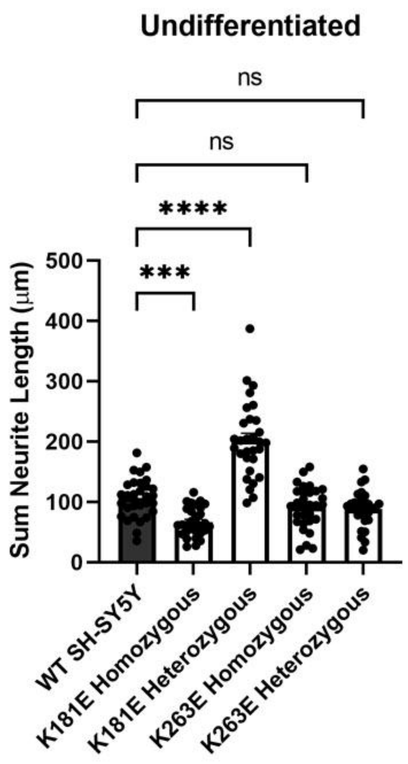
Undifferentiated
Sum Neurite Length (μm)
WT SH-SY5Y
K181E Homozygous
K181E Heterozygous
K263E Homozygous
K263E Heterozygous

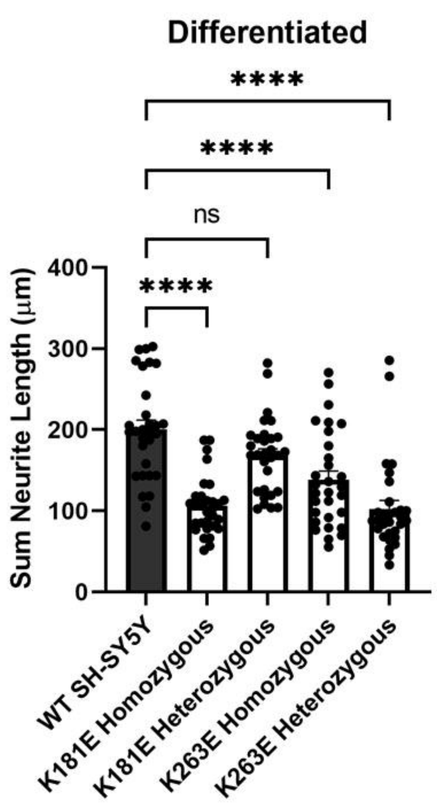
Differentiated
Sum Neurite Length (μm)
WT SH-SY5Y
K181E Homozygous
K181E Heterozygous
K263E Homozygous
K263E Heterozygous

E)

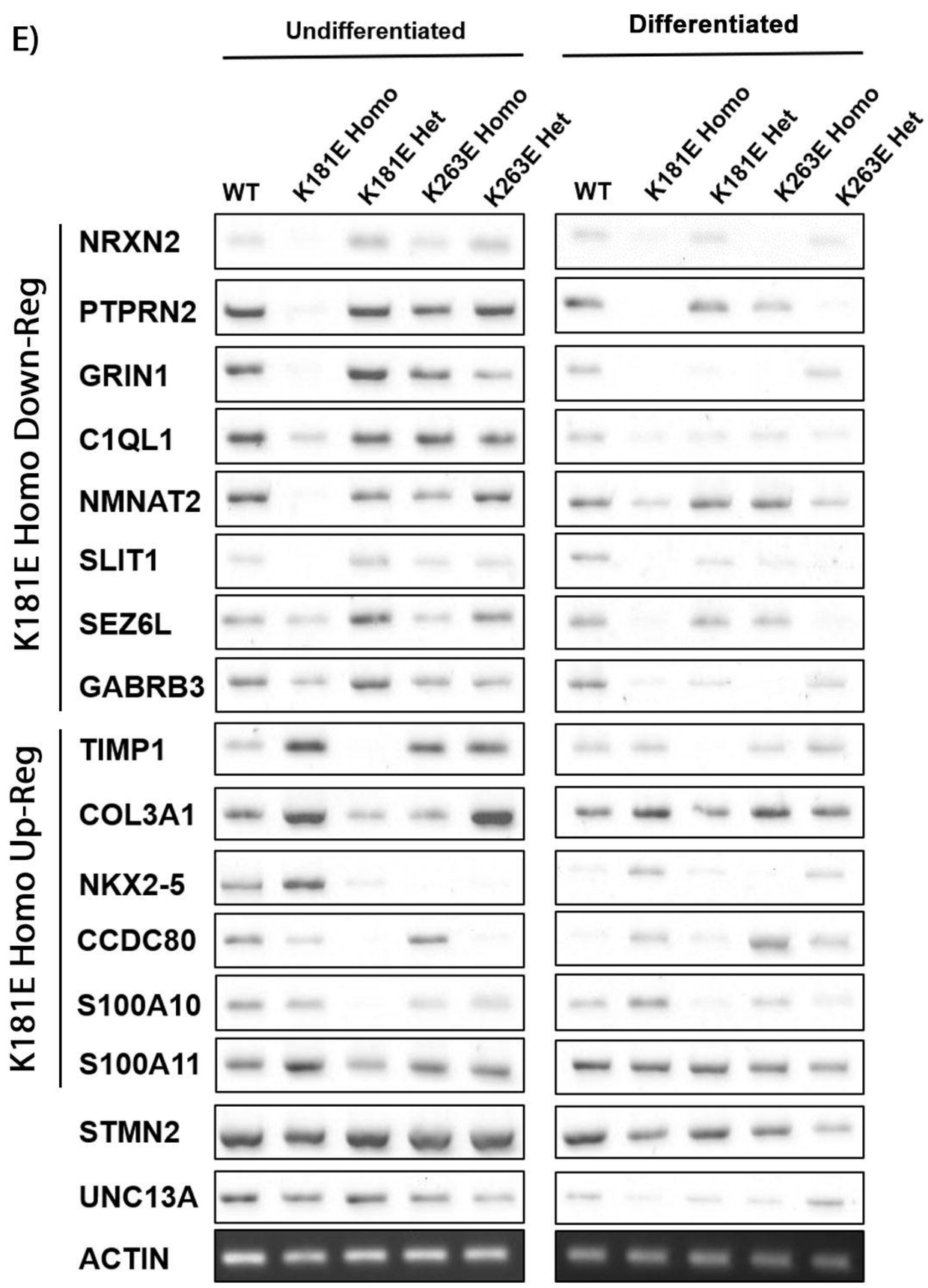
Undifferentiated
Differentiated
WT
K181E Homo
K181E Het
K263E Homo
K263E Het
K181E Homo Down-Reg
NRXN2
PTPRN2
GRIN1
C1QL1
NMNAT2
SLIT1
SEZ6L
GABRB3
K181E Homo Up-Reg
TIMP1
COL3A1
NKX2-5
CCDC80
S100A10
S100A11
STMN2
UNC13A
ACTIN